Doctoral Dissertation

Development of heat-resistant interconnections for wide bandgap semiconductor power modules

Seungjun Noh

January 2019

Department of Adaptive Machine Systems
Graduate school of Engineering
Osaka University

Ph.D. Dissertation

Development of heat-resistant interconnections for wide bandgap semiconductor power modules

by

Seungjun Noh

Department of Adaptive Machine Systems

Graduate school of Engineering

Osaka University

January 2019

Approved by

Professor Katsuaki Suganuma

Professor Yoritoshi Minamino

Associate Professor Shijo Nagao

Associate Professor Tohru Sugahara

Development of heat-resistant interconnections for wide bandgap semiconductor power modules

Abstract

The development of wide-bandgap (WBG) semiconductors, such as SiC and GaN, provides a significant opportunity to explore next-generation power electronic systems that possess increased power density, operating frequency, and break-down voltage. One of the main challenges in WBG semiconductor technology is the high associated operating temperature, which can be in excess of 250 °C. Because the contemporary, established interconnection materials that are used for Si semiconductors cannot be operated continuously at temperatures above 150 °C, the development of novel interconnection materials, including suitable metallization, is an urgent requirement for WBG semiconductors applied in severe thermal environments. This thesis describes heat-resistant interconnection materials for use in wire interconnection and in die-attach.

At first, a heat-resistant wire interconnection was introduced, realized by printing Ag sinter paste. Both the high-temperature reliability and high-current reliability of the Ag paste as the wire interconnection were evaluated using an aging test at 250 °C for 1000 h and an electromigration test at 2.2×10^4 A/cm^2 for 2000 h. In the aging test, a resistivity of approximately 4.1×10^{-6} Ω cm was achieved, which further decreased to 3.4×10^{-6} Ω cm after aging for 1000 h. This reduction could be attributed to further sintering of the sintered Ag network. The initial shear strength was 17 MPa. While high enough, this value was maintained even after an aging test of 1000 h. In the EM test, the resistance of the Ag paste wire interconnection did not change significantly up to the 1000 h mark and then increased only slightly at 2000 h. This slight change in resistance demonstrates higher stability than that of conventional wire interconnection materials, such as Al and Cu, under high temperature and high current density conditions.

Heat-resistant die-attacht involving the use of cold-rolled Ag sheets was then developed. The reduction ratios of 0%, 66%, 80%, and 90% were evaluated. The cold rolling of the Ag sheet induced grain refinement down to a sub-micron level along with high, associated residual stress, which was the driving force for hillock growth on the Ag sheet. This resulted in intimate bonding. With an increasing reduction ratio, the shear strength increased to approximately 20 MPa. This could be attributed to decreased grain size due to the cold rolling, which provided an increase in Ag atom migration pathways for hillock formation. TEM observations confirmed that the Ag nanoparticles were generated between two hillocks with a specified growth direction, leading to an interface bonding between the two Ag films.

Finally, for applications involving large-area die-attacht, the possibility of using Ag stress migration bonding technology was confirmed. Hillock growth change was observed on the Ag layer under various bonding conditions. The variation in the hillock growth area and the associated relationship with bonding strength were noted. A large bonded area (20 x 20 mm) was achieved using an Ag stress migration bonding process, resulting in an average flexural strength of 40.5 MPa at 300 °C. In-situ stress analysis during heating confirmed that compressive thermal stress was generated because of the coefficient of thermal expansion (CTE) mismatch at the Ag layer/substrate interface. The stress was released in over the bonding areas in which the temperature was approximately 100 °C. The relaxation of residual stress was caused by the formation of abnormal silver hillocks. The bonding strength in various areas indicated that the hillock growth could have occurred homogeneously over the entire bonding area.

In this study, the results confirmed that the developed heat-resistant interconnection materials could become potential alternative interconnection technologies for next-generation power electronic devices.

Table of contents

List of tables

List of figures

Chapter 1

Introduction

1.1 Requirements of interconnection materials for high temperature applications

1.1.1 Next generation wide band-gap power electronic devices

As compared to conventional silicon (Si) semiconductors, the wide band-gap (WBG) semiconductors, such as silicon carbide (SiC) and gallium nitride (GaN), have been widely studied because of the expected increase in power density, operating frequency, and breakdown voltage owing to their intrinsic properties [1–3]. The physical properties of Si and wide band-gap semiconductors are listed in Table 1.1 [3].

Table 1.1 Physical properties of Si and wide band-gap semiconductors [3].

	Si	3H–SiC	6H–SiC	4H–SiC	GaN	Diamond
Bandgap energy, E_g (eV)	1.12	2.3	2.9	3.2	3.4	5.6
Electron mobility, μ_n ($cm^2\ V^{-1}\ S^{-1}$)	1450	1000	415	950	2000	4000
Hole mobility, μ_p ($cm^2\ V^{-1}\ S^{-1}$)	450	45	90	115	350	3800
Critical electric field, E_c ($V\ cm^{-1}$)	3×10^5	2×10^6	2.5×10^6	3×10^6	5×10^6	10^7
Saturation velocity, v_{sat} ($cm\ s^{-1}$)	10^7	2.5×10^7	2×10^7	2×10^7	2×10^7	3×10^7
Thermal conductivity, λ ($W\ cm^{-1}\ K^{-1}$)	1.3	5	5	5	1.3	20
Dielectric constant, ε_r	11.7	9.6	9.7	10	8.9	5.7

The performance characteristics of power electronics can be significantly improved by using WBG semiconductors although an increase in power density leads to higher operating temperatures (> 250 °C). This will also allow a substantial volume and weight reduction of the device. In addition, the use of WBG semiconductors has resulted in a significant improvement in the operating-voltage range for power devices along with the switching speed

and/or specific on resistance [1]. Therefore, WBG semiconductors can be widely used in applications such as high-speed railways, electric/hybrid vehicles, and 5th generation communication systems. Fig. 1.1 shows power switching applications in mid- to high-power conversion. WBG semiconductors can replace the current Si-based insulated gate bipolar transistor (IGBT), allowing the device to operate under higher temperature conditions and at higher current densities.

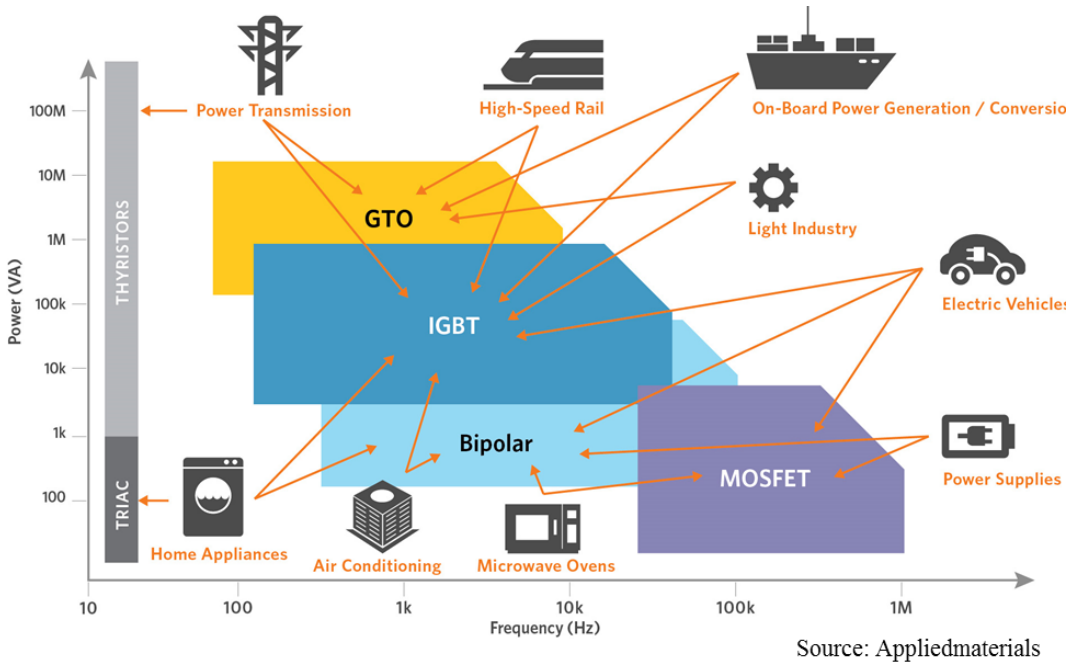

Fig. 1.1 Power switching applications in mid- to high-power conversion.

For application of WBG semiconductors in electric vehicles (EVs) and hybrid electric vehicles (HEVs), junction temperatures (Tj) above 200 °C can be expected [4]. Because the current interconnection materials that have been established for Si semiconductors only operate at temperatures of up to 150 °C, the development of novel heat-resistant interconnection materials is required for operation beyond 200 °C.

1.1.2 Requirements for high temperature die-attachment

Die-attach structures in power electronic devices consist of a semiconductor die, die-attach material, and a substrate with a metallization layer, which all have different associated thermal and mechanical properties. Severe thermal stress can be generated by a mismatch in these components at elevated temperatures, leading to device failure [5]. To ensure the high performance and reliability of WBG power electronic devices at high temperatures and currents, the die-attach and wiring materials both need to possess the following characteristics:

1. Die-attach materials must withstand high operating temperatures (>250 °C) and provide excellent reliability for the package structure [6].
2. Thermomechanical stresses generated by coefficient of thermal expansion (CTE) mismatches between the device components at high temperature must be compensated for [7].
3. The metallization of the semiconductor die and substrate must be optimized because certain die-attach materials may need a specific metallization to achieve good bonding and compatibility at elevated temperatures [8].
4. Die attach materials must possess high electrical conductivity and high thermal conductivity to dissipate the substantial heat flux originating from the operation of the power semiconductors [9].

Conventional die-attach materials, such as Pb-based solders and Sn-Ag and Sn-Ag-Cu solders with melting points below 300 °C, that are typically used for Si power electronics are not suitable for WBG power devices because of their poor reliability at high temperatures [10–12]. These conventional solders have disadvantages such as the formation of liquid, the growth of brittle intermetallic compounds (IMCs), and voiding even at standard operating

temperatures. Fig. 1.2a shows scanning electron microscopy (SEM) images of the interfacial microstructures of die-attach using the Pb-5Sn solder [13]. After the thermal shock test (-40 °C to 125 °C for 2000 cycles), many cracks were formed at the interface between the Pb-5Sn solder and the Cu3Sn IMC layer, as shown in Fig. 1.2b. In addition to high temperature degradation, environmental regulations in regard to Pb-free products have become mandatory requirements [14]. To realize all the advantages of WBG semiconductors, the development of high temperature die-attach must be accomplished as the first technological step toward solving the packaging bottleneck.

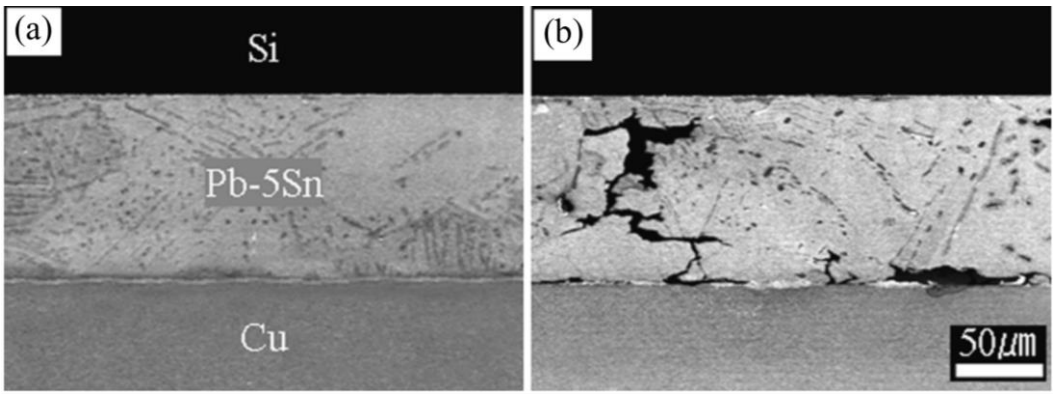

Fig. 1.2 SEM images of the interfacial microstructures of the die-attach using the Pb-5Sn solder (a) under initial condition and (b) after the thermal shock test (-40 ℃ to 125 ℃ for 2000 cycles) [13].

1.1.3 Requirements for high temperature wire interconnections

Ribbon and wire bonding have typically been used for the wiring of power electronic devices. To ensure the high-performance and reliability of WBG semiconductor power devices, the following characteristics are required for wire interconnection materials.

1. They must allow high current densities at high operating temperatures and must possess good electrical properties. The electrical resistivity should not increase with changing temperature.
2. Electromigration (EM), which is one of the serious concerns caused by increasing current density, must be minimized [15].
3. Wire interconnection materials must withstand high operating temperatures of up to 250 °C. Conventional wiring materials such as Cu and Al easily form IMCs at high temperatures, which degrades their current-carrying capacity.
4. Thermomechanical stresses, generated both in bond formation using ultrasonic processes and by CTE mismatches between the device components, must be minimized [16].

In this regard, conventional wiring materials such as Cu and Al raise serious concerns in relation to reliability at high temperatures and currents. Cu wiring requires special care, such as the use of a reduction gas or coatings for bonding, because of the formation of Cu oxide at relatively low temperatures [17]. Fig. 1.3a shows a TEM image of the interface between the Cu wire and Al metallization after aging at 175 °C for 100 h. The growth of CuAl2 and Cu9Al4 (Fig. 1.3a, b) was observed even after aging at 175 °C, which led to cracking or interface failure [18]. High-purity Al wire has already been used in power devices because of its excellent formability in the wiring process. However, high-purity Al raises reliability concerns because of its rapid grain-coarsening and relatively low current/heat conductivity when operating at high temperatures [19]. Fig. 1.4 shows the typical failure locations

associated with Al wire bonding when subjected to thermal shock [20]. Furthermore, EM is also one of the main risks for Cu and Al at high currents [21].

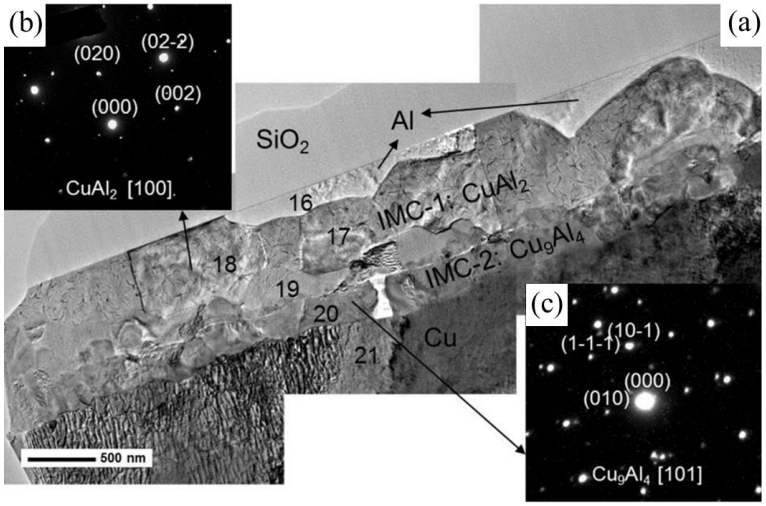

Fig. 1.3 (a) TEM image of the Cu–Al interface after aging at 175 °C for 100 h; (b) SAED with $CuAl_2$; and (c) SAED with Cu_9Al_4 [18].

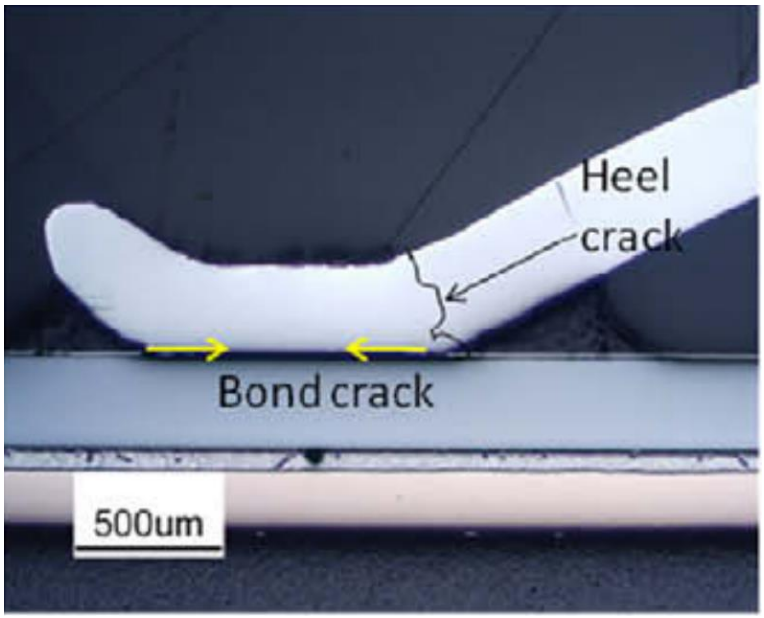

Fig. 1.4 Typical failure locations of Al wire bonding under thermal stress [20].

1.2 Interconnection material candidates for high temperature applications

1.2.1 Silver sinter paste

To ensure the high performance and reliability of WBG power devices operated at high temperatures, Ag nanoparticle (AgNP) pastes prepared by low-temperature sintering have drawn considerable attention for use as potential die-attach materials. This is due to their high melting point, high electrical conductivity, and their high thermal conductivity [22, 23]. Fig. 1.5 shows schematics of sintering parameters such as particle size, pressure, time, temperature, and surface condition of substrates. The device components are generally assembled under high pressure applied to the AgNP paste for specific time periods and at specific temperatures, as shown in Fig. 1.5a. The properties of the bonded joints are influenced by two types of interface: nanoparticle-nanoparticle interfaces and nanoparticle-substrate interfaces, as shown in Fig. 1.5b, c. The die attach using the AgNP pastes was formed by sintering in air at 200 °C to 300 °C with an applied pressure ranging between 0 and 40 MPa [24]. AgNPs are generally mixed with binders, solvents, and dispersants in order to disperse the nanoparticles to maintain the disiable Ag content and viscosity [25]. However, because of the large specific surface area of AgNPs, a substantial amount of the dispersant and the binder remains in the sinter AgNP pastes. This residue sometimes inhibits sintering of AgNPs [26]. Table 1.2 summarizes the developed AgNP paste with its typical sintering parameters for WBG application.

Microsized Ag pastes have been introduced as an alternative to AgNPs as high-temperature die-attach materials. Bonding with microsized Ag paste can be performed with a relatively low applied pressure of 0.4 MPa [27]. Because Ag microflakes do not tend to aggregate, protective dispersants are not required. In addition, Zang et al. reported the low-temperature, pressure-less sintering of microsized Ag paste [28]. They used Ag

microflake paste mixed with Ag2O particles, which were reduced in-situ to AgNPs to activate the surface of the Ag microparticles, resulting in a stable bonding structure at 180 °C. Suganuma et al. reported the excellent performance of a low-pressure low-temperature sinter joint using a hybrid paste of microsized Ag and submicron-sized Ag [9]. The assembled device exhibited excellent stability under thermal shock testing at a temperature range of -40 °C to 300 °C in air. Table 1.3 summarizes the developed microsized Ag pastes and the hybrid Ag particle paste with its typical sintering parameters for WBG application.

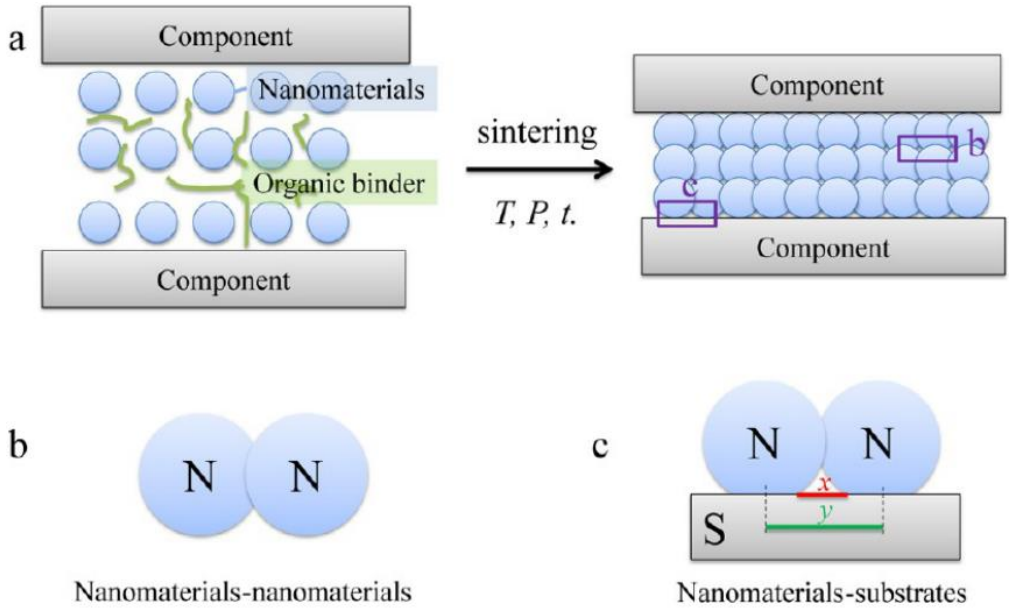

Fig. 1.5 (a) Bonding schematic for sintered nanomaterial fillers: T, P, and t are sintering temperature, pressure, and time, respectively. Interface qualities of (b) nanomaterials-nanomaterials and (c) nanomaterials-substrates in terms of the joint properties (x is the uncovered length, and y is the distance between the centers of the two NPs) [24].

Table 1.2 The developed AgNP paste with its typical sintering parameters for WBG application.

Die attach materials		Sintering parameters			Property	Ref
Size (nm)	Bonding substrate	Temperature (℃)	Time (min)	Pressure (MPa)	Shear strength (MPa)	
3-20	Cu discs	300	5	5	25-40	[29]
20-100	Cu wire to Cu foil	300	30	5	21.9	[30]
40	Ag-coated Cu plates	250	30	5	40	[31]
Commercial paste	Si to DBC	240	5	40	-	[32]
10	Cu discs	250	3	10	30	[33]
Commercial paste	Ag-coated Cu plates	275	20	5	31.6	[34]
20-168	Cu discs	250	5	0	13.7	[35]
20-80	Cu plates	200	20	0	25	[36]

Table 1.3 The developed micron size Ag particle paste and hybrid Ag particle paste with its typical sintering parameters for WBG application.

Die attach materials		Sintering parameters			Property	Ref
Size (μm)	Bonding substrate	Temperature (℃)	Time (min)	Pressure (MPa)	Shear strength (MPa)	
3 (chestnut-burr)	ENIG-coated Cu discs	300	10	10	> 30	[37]
8 (flake)	Ag-coated SiC to DBC	300	60	0.4	37	[27]
8 (flake), 0.3 (sphere) (ratio 90 : 10)	Ag-coated SiC to DBC	300	60	0.7	< 40	[9]
6 (flake), 3 (Ag2O) (ratio 90 : 10)	Ag-coated Cu plates	180	40	0	42	[28]
6 (flake), 0.6 (SiC) (ratio 98 : 2)	Ag-coated Cu plates	250	30	0.4	35	[38]

1.2.2 Low-temperature Ag sintering mechanism

Recently, the low-temperature sintering mechanism of microsized Ag particles was investigated in a study on Ag film-to-film bonding, which was termed stress migration bonding (SMB). SMB is achieved through a reaction described as the "nano-volcanic eruption of Ag" which is caused by stress migration accompanied by oxygen absorption and reaction with Ag at temperatures of approximately 200 °C [39–43]. Fig. 1.6 schematically depicts the Ag nano-volcanic-eruption-assisted formation of an amorphous Ag film, an abundant Ag hillock, a patterned Ag hillock array, and an Ag/Ag joint [44]. The free surfaces and grain boundaries of the Ag film readily absorb oxygen at elevated temperatures (Fig. 1.6a). By application of the thermodynamic calculation, it was found that oxygen absorbed in the Ag columnar grain boundary could form an Ag-O fluid at approximately 200 °C (Fig. 1.6b). The liquid Ag-O could be squeezed out of the grain boundaries of the Ag film to the surface under compressive stress (Fig. 1.6c). The released Ag-O immediately formed amorphous Ag-O that was deposited on the Ag film surface (Fig. 1.6d) and the Ag-O was reduced to form Ag nanoparticles at this temperature (Fig. 1.6e and f). During the subsequent heat treatment, Ag hillocks were continuously formed (Fig. 1.6g1), resulting in the formation of strong Ag/Ag joints (Fig. 1.6g3). This phenomenon has been confirmed by high resolution TEM observation, and the related research results have been published, as shown in Fig. 1.7 [44]. Thus, the SMB process can be applicable to a wide range of heat/electric-conductive interconnections including next generation power devices.

The basic low temperature sintering mechanism was identical to the sintering process for the hybrid Ag paste mentioned previously. Ag flakes and particles absorbed oxygen along the grain boundaries and similar defects in the particles/flakes. This absorption process led to the formation of liquid followed by the nano-volcanic eruption of Ag. This reaction enhanced the sintering of the particles/flakes at approximately 200 °C in air.

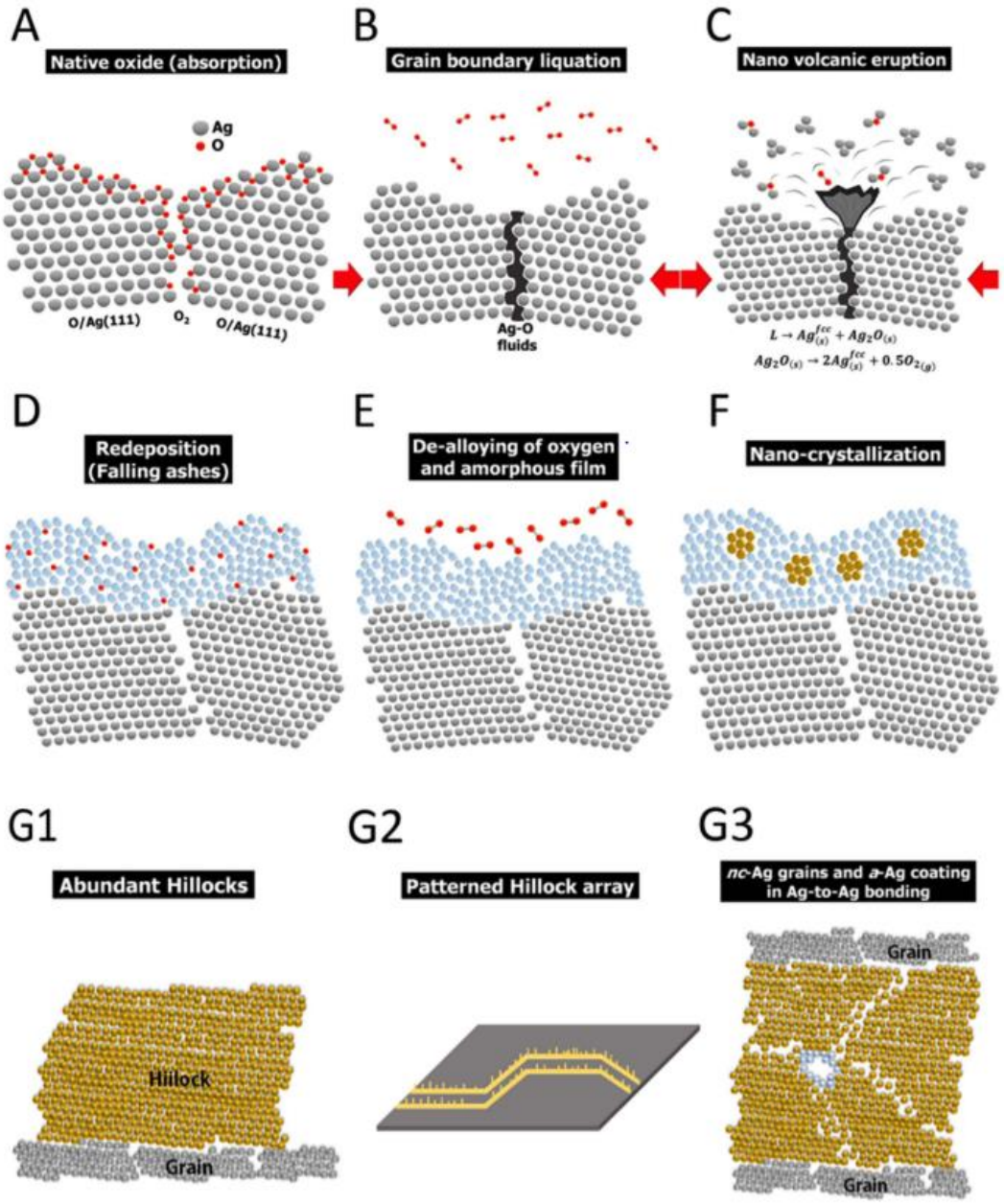

Fig. 1.6 Schematic diagram of an Ag nano-volcanic eruption: (a) Native oxide, (b) grain boundary liquation, (c) nano-volcanic eruption of Ag and Ag2O clusters and O2 gas, (d) re-deposition of Ag-O coating, (e) de-alloying of O and formation of amorphous Ag film, (f) homogeneous nucleation of nanocrystalline Ag grains, and formation of (g1) abundant Ag hillocks, (g2) a number of Ag hillock arrays, or (g3) strong [44].

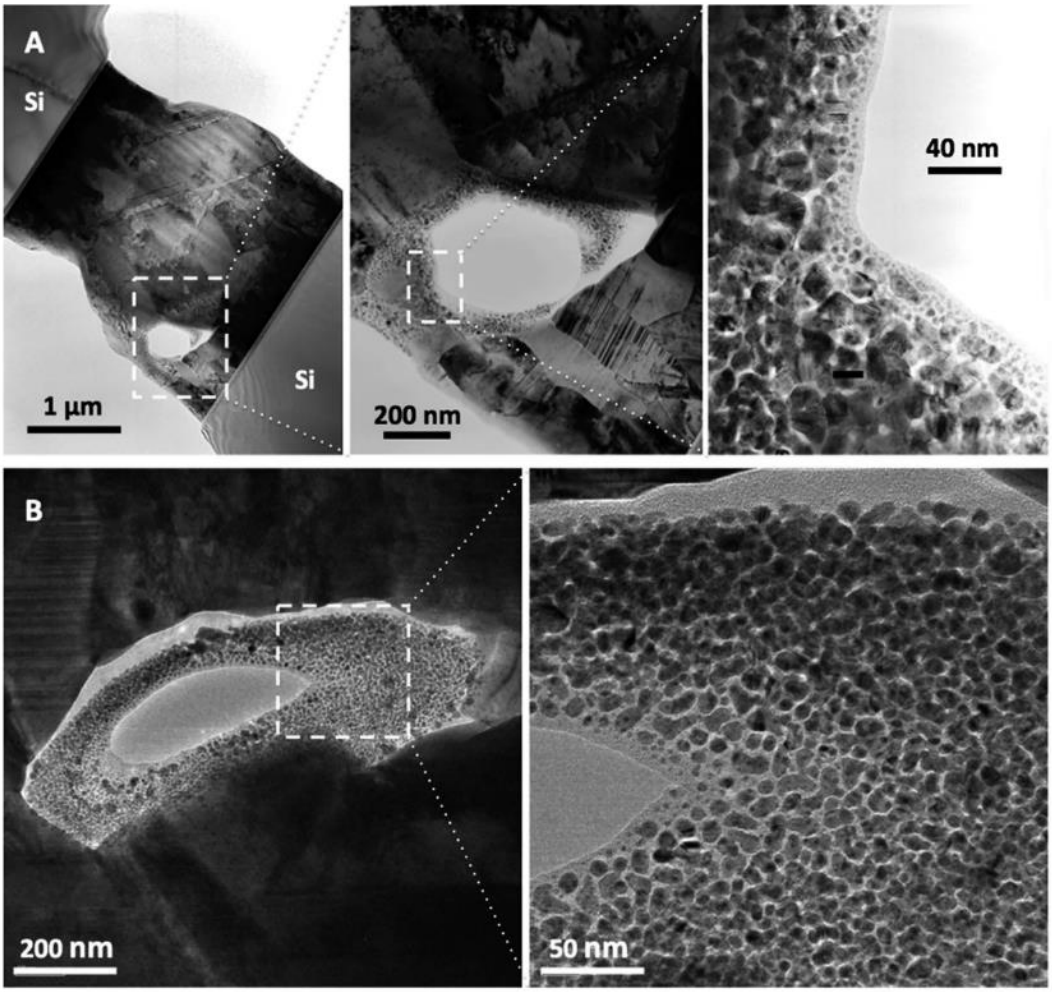

Fig. 1.7 Cross-sectional TEM images of a Ag/Ag joint bonded using 1-μm-thick sputtered Ag films at 250 °C under the ambient atmosphere for 1 h: (a) overview and close-up images of a joint and (b) overview and close-up image of the other joint [44].

1.2.3 Transient liquid phase bonding

Transient liquid phase (TLP) bonding is one of the candidates for high-temperature die-attach. In the bonding process, a low melting-point interlayer between the base metals is bonded together in the die-attach structure by isothermal solidification at the bonding temperature [45–47]. During heating, a low melting-point interlayer melts and begins to react with the base metals to form IMCs which can withstand high operating temperatures. The schematic diagram of the TLP bonding process is shown in Fig. 1.8 [48]. The bonding processes are divided into six stages:

1. Initial condition (Fig. 1.8a)
2. Dissolution (Fig. 1.8b)
3. Isothermal solidification (Fig. 1.8c)
4. Completion of isothermal solidification (Fig. 1.8d)
5. Solid state homogenization (Fig. 1.8e
6. Final condition (Fig. 1.8f)

Elements with low melting points, such as Sn and In, have typically been used as an interlayer for TLP bonding. TLP systems including Au/In [45], Ag/In [22], [49], Au/Sn [50, 51], and Cu/Sn [52] have been reported as candidates for die-attach in power electronics. Mustain et al. reported TLP achieved using the Ag/In and Au/In systems for high temperature applications. After TLP was achieved with Ag/In system soldering, two inter-metallic phases of AgIn2 and Ag2In were formed in the pure Ag. It was found that after thermal exposure at 400 °C for 100 h, the uniformity of the TLP bonding was enhanced, and TLP bonding became more homogeneous because of the continuous formation of the Ag–In IMCs, resulting in an increase in bonding strength. TLP soldering was also examined in the case of the Au-12%Ge solder for die-attach of SiC. The die attach was formed at 400 °C and possessed good stability

at 300 °C [22]. TLP bonding has several advantages such as high temperature sustainability and reasonable cost; however, it possesses limitations such as the formation of brittle IMCs or Kirkendall voids at the bonding interface when exposed to thermal shock.

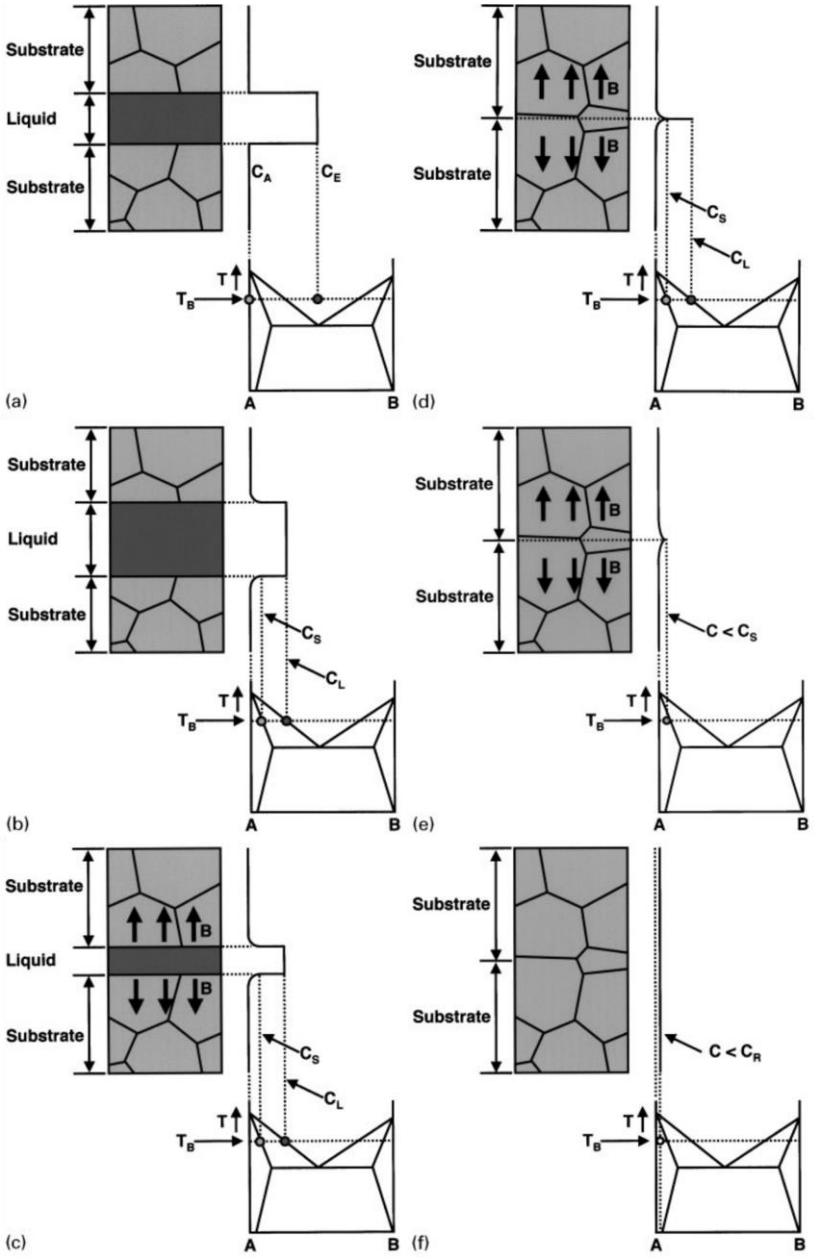

Fig. 1.8 Schematic diagrams of (a) initial condition: (b) dissolution; (c) isothermal solidification; (d) completion of isothermal solidification; (e) solid state homogenization; (f) final condition [48].

1.2.4 Ribbon bonding

Al and Cu ribbon bonding performed using ultrasonic methods has been attracting much attention for its potential to address high current interconnection requirements [53]. It possesses excellent electrical advantages, such as higher current capacity and lower impedance when compared with Al wire bonding. Fig. 1.9 shows a schematic of the electrical resistance characteristic for a rectangular ribbon and a round wire [16]. The current capacity of ribbons is significantly improved because of their width and associated cross-sectional area in comparison with round wires. This can be an important role for high power modules [54, 55].

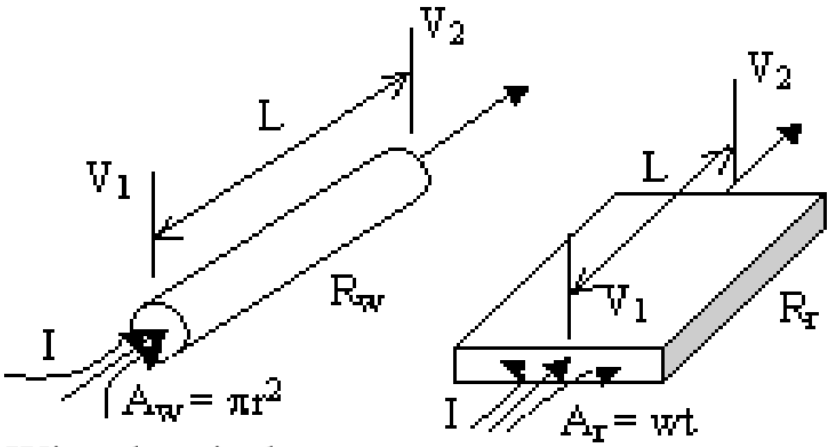

Wire electrical resistance:

$$R_w = \frac{\rho L}{A_w} = \frac{\rho L}{\pi r^2}$$

Ribbon electrical resistance:

$$R_r = \frac{\rho L}{A_r} = \frac{\rho L}{wt}$$

ρ =material resistivity

Fig. 1.9 Wire and ribbon form factor for the determination of electrical resistance [16].

In addition, because the geometry of multiple wires sometimes possesses a non-uniform bonding face, an inhomogeneous heat distribution and associated thermal stress may be generated on the bonding face of the semiconductors when high current is applied. High

power devices can endure high currents by using large uniform ribbon bonds rather than by multiple wire bonds. However, Al ribbon raises reliability concerns because of its rapid grain coarsening and relatively low current/heat conductivity at high temperatures. Heel crack formation due to exposure to thermal shock is also one of the main risks associated with the use of Al ribbon.

Park et al. reported ribbon bonding with a Cu/Al clad ribbon for high temperature applications, as shown in Fig. 1.10 [56]. They used a Cu/Al clad ribbon (Fig 1.10a) to bond an electroless nickel immersion gold (ENIG)-finished Cu substrate (Fig. 1.10b) to enhance the mechanical and electrical properties. A high-temperature exposure test at 200 ℃ and a thermal shock test performed within a range of -40 ℃ to 250 ℃ revealed its excellent stability in comparison with the performance of pure Al ribbon bonding under high temperature testing. Some of the limitations of ribbon bonding using Al and Cu include the formation of brittle IMC or of heal crack, that results in the degradation of the reliability of power devices.

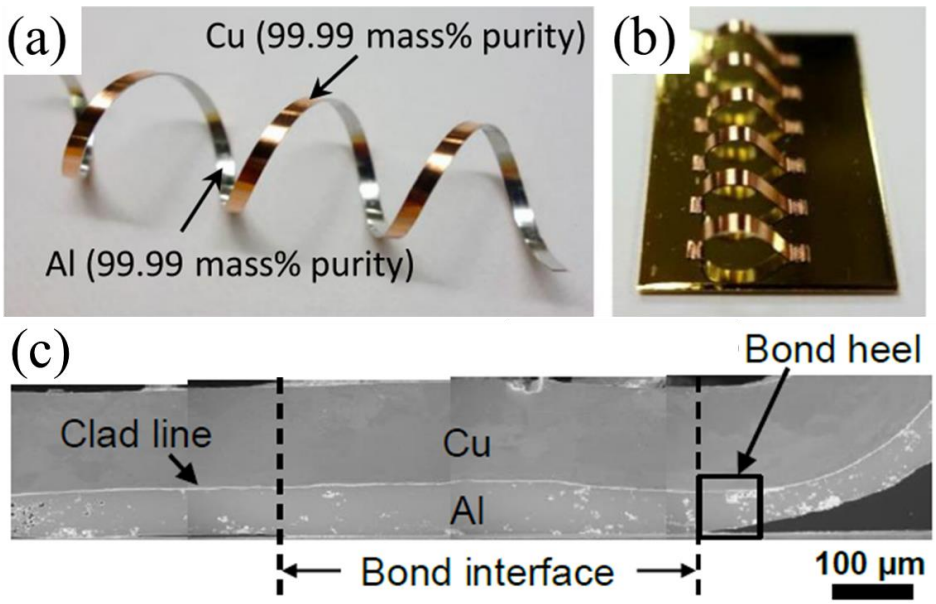

Fig. 1.10 Schematics of (a) cold-rolled Cu/Al clad ribbon; (b) wiring samples; and (c) cross sectional SEM image of Cu/Al clad ribbon bonding [56].

1.3 Objective and outline of the thesis

As mentioned in the preceding sections, WBG power devices have demonstrated excellent potential for enhancing high-temperature performance. To ensure long-term reliability in severe thermal environments, the interconnection materials must be studied both for die-attach and for wiring. The main purpose of the current study as presented in this thesis is the development of heat-resistant interconnection materials involving wire interconnection and die-attach.

In Chapter 1, brief descriptions on the background of power electronics and emerging issues related to the use of WBG semiconductors are introduced. The current candidates for interconnection materials, including those for use in die-attach, wire, and their interfaces, are also introduced.

In Chapter 2, printed wire interconnection using the Ag sinter paste is proposed as a novel wire bonding solution for use under high temperature and high current conditions. Use of the Ag paste can improve long-term reliability because of its high melting point and intrinsically excellent electrical and thermal conductivity. The long-term reliability of the Ag sinter paste wires is compared to that of Al ribbons by conducting harsh environmental tests, such as an aging test at 250 °C and an electromigration test at 2.2 × 104 A/cm2. It is proposed that the interfacial degradations in the Ag sinter paste wire, such as brittle intermetallic phases and corrosion, can be prevented by the use of the same materials in both the wire and metallization layer.

In Chapter 3, a heat-resistant die-attach using a cold-rolled Ag sheet is developed based on Ag stress migration bonding. Hillock and whisker growth are commonly observed on the Si or metal substrate of coated metallic films because of the stress-migration induced by a CTE mismatch. However, in the case of a metal sheet, hillock growth is rarely reported

because of the lack of driving force for stress migration. Here, hillock growth on the Ag sheet was optimized by cold-rolling to achieve interface bonding between the sheet and the sputtered films. In particular, the detailed mechanism underlying hillock joining is investigated.

In Chapter 4, with increasing demand for high power density in WBG-semiconductor-based power electronics, large-area die-attach (20 × 20 mm) using Ag stress migration bonding is discussed. Observations of how the hillock growth changes on the Ag layer under various bonding conditions are made. In particular, the details of how it varies over large areas, and how this variation is related to the bonding strength are investigated. The evolution of in-situ residual stresses in the entire substrate area during the heating and cooling process is also discussed.

In Chapter 5, a summary of the heat-resistant interconnection materials is presented. These materials can be acknowledged as alternative interconnection technologies for next-generation power electronic devices.

Reference

[1] J. Biela, M. Schweizer, S. Waffler, and J. W. Kolar, “SiC versus Si - Evaluation of potentials for performance improvement of inverter and DCDC converter systems by SiC power semiconductors,” IEEE Transactions on Industrial Electronics, vol. 58, no. 7, pp. 2872–2882, 2011.

[2] J. L. Hudgins, G. S. Simin, E. Santi, and M. A. Khan, “An assessment of wide bandgap semiconductors for power devices,” IEEE Transactions on Power Electronics, vol. 18, no. 3, pp. 907–914, 2003.

[3] C. Buttay et al., “State of the art of high temperature power electronics,” Materials Science and Engineering B: Solid-State Materials for Advanced Technology, vol. 176, no. 4, pp. 283–288, 2011.

[4] S. Tanimoto and H. Ohashi, “Reliability issues of SiC power MOSFETs toward high junction temperature operation,” Physica Status Solidi (A) Applications and Materials Science, vol. 206, no. 10, pp. 2417–2430, 2009.

[5] C. Chen et al., “Mechanical Deformation of Sintered Porous Ag Die Attach at High Temperature and Its Size Effect for Wide-Bandgap Power Device Design,” Journal of Electronic Materials, vol. 46, no. 3, pp. 1576–1586, 2017.

[6] V. R. V. R. Manikam and K. Y. K. Y. K. Y. Cheong, “Die Attach Materials for High Temperature Applications: A Review,” IEEE Transactions on Components, Packaging and Manufacturing Technology, vol. 1, no. 4, pp. 457–478, 2011.

[7] A. A. Bajwa, Y. Qin, R. Reiner, R. Quay, and J. Wilde, “Assembly and Packaging Technologies for Higherature and High-Power GaN Devices,” IEEE Transactions on Components, Packaging and Manufacturing Technology, vol. 5, no. 10, pp. 1402–1416, 2015.

[8] H. Zhang, S. Nagao, K. Suganuma, H. J. Albrecht, and K. Wilke, "Thermostable Ag die-attach structure for high-temperature power devices," Journal of Materials Science: Materials in Electronics, vol. 27, no. 2, pp. 1337–1344, 2016.

[9] K. Suganuma, S. Sakamoto, N. Kagami, D. Wakuda, K. S. Kim, and M. Nogi, "Low-temperature low-pressure die attach with hybrid silver particle paste," Microelectronics Reliability, vol. 52, no. 2, pp. 375–380, 2012.

[10] K. S. Kim, C. H. Yu, N. H. Kim, N. K. Kim, H. J. Chang, and E. G. Chang, "Isothermal aging characteristics of Sn-Pb micro solder bumps," Microelectronics Reliability, vol. 43, no. 5, pp. 757–763, 2003.

[11] T. Laurila, V. Vuorinen, and J. K. Kivilahti, "Interfacial reactions between lead-free solders and common base materials," Materials Science and Engineering R: Reports, vol. 49, no. 1–2, pp. 1–60, 2005.

[12] L. N. Ramanathan, J. W. Jang, J. K. Lin, and D. R. Frear, "Solid-state annealing behavior of two high-Pb solders, 95Pb5Sn and 90Pb10Sn, on Cu under bump metallurgy," Journal of Electronic Materials, vol. 34, no. 10, pp. 43–46, 2005.

[13] S. Kim, K. S. Kim, S. S. Kim, K. Suganuma, and G. Izuta, "Improving the reliability of Si die attachment with Zn-Sn-based high-temperature Pb-free solder using a TiN diffusion barrier," Journal of Electronic Materials, vol. 38, no. 12, pp. 2668–2675, 2009.

[14] K. Suganuma, "Advances in lead-free electronics soldering," Current Opinion in Solid State and Materials Science, vol. 5, no. 1, pp. 55–64, 2001.

[15] B. Krabbenborg, "High current bond design rules based on bond pad degradation and fusing of the wire," Microelectronics Reliability, vol. 39, no. 1, pp. 77–88, 1999.

[16] B. Ong, M. Helmy, S. Chuah, C. Luechinger, and G. Wong, "Heavy Al Ribbon

Interconnect: An Alternative Solution for Hybrid Power Packaging," Imaps, no. November, pp. 1–11, 2004.

[17] H. Xu, I. Qin, H. Clauberg, B. Chylak, and V. L. Acoff, "Behavior of palladium and its impact on intermetallic growth in palladium-coated Cu wire bonding," Acta Materialia, vol. 61, no. 1, pp. 79–88, 2013.

[18] H. Xu et al., "Behavior of aluminum oxide, intermetallics and voids in Cu-Al wire bonds," Acta Materialia, vol. 59, no. 14, pp. 5661–5673, 2011.

[19] M. Schneider-Ramelow and C. Ehrhardt, "The reliability of wire bonding using Ag and Al," Microelectronics Reliability, vol. 63, pp. 336–341, 2016.

[20] H. Lu, C. Bailey, and C. Yin, "Design for reliability of power electronics modules," Microelectronics Reliability, vol. 49, no. 9–11, pp. 1250–1255, 2009.

[21] T. Hashimoto, K. Fujito, K. Samonji, J. S. Speck, and S. Nakamura, "Electromigration failure modes in aluminum metallization for semiconductor devices," Proceedings of the IEEE, vol. 57, no. 9, pp. 1587–1594, 1969.

[22] R. Kisiel and Z. Szczepański, "Die-attachment solutions for SiC power devices," Microelectronics Reliability, vol. 49, no. 6, pp. 627–629, 2009.

[23] J. G. Bai, J. N. Calata, G. Lei, and G. Q. Lu, "Thermomechanical reliability of low-temperature sintered silver die-attachment," Thermomechanical Phenomena in Electronic Systems -Proceedings of the Intersociety Conference, vol. 2006, no. 3, pp. 1126–1130, 2006.

[24] P. Peng, A. Hu, A. P. Gerlich, G. Zou, L. Liu, and Y. N. Zhou, "Joining of Silver Nanomaterials at Low Temperatures: Processes, Properties, and Applications," ACS Applied Materials and Interfaces, vol. 7, no. 23, pp. 12597–12618, 2015.

[25] K. S. Siow, "Are sintered silver joints ready for use as interconnect material in

microelectronic packaging?," Journal of Electronic Materials, vol. 43, no. 4, pp. 947–961, 2014.

[26] K. Qi, X. Chen, and G.-Q. Lu, "Effect of interconnection area on shear strength of sintered joint with nano-silver paste," Soldering & Surface Mount Technology, vol. 20, no. 1, pp. 8–12, 2008.

[27] S. Sakamoto, S. Nagao, and K. Suganuma, "Thermal fatigue of Ag flake sintering die-attachment for Si/SiC power devices," Journal of Materials Science: Materials in Electronics, vol. 24, no. 7, pp. 2593–2601, 2013.

[28] H. Zhang, Y. Gao, J. Jiu, and K. Suganuma, "In situ bridging effect of Ag2O on pressureless and low-temperature sintering of micron-scale silver paste," Journal of Alloys and Compounds, vol. 696, pp. 123–129, 2017.

[29] S. Wang, H. Ji, M. Li, and C. Wang, "Fabrication of interconnects using pressureless low temperature sintered Ag nanoparticles," Materials Letters, vol. 85, pp. 61–63, 2012.

[30] H. Alarifi, A. Hu, M. Yavuz, and Y. N. Zhou, "Silver nanoparticle paste for low-temperature bonding of copper," Journal of Electronic Materials, vol. 40, no. 6, pp. 1394–1402, 2011.

[31] J. Yan et al., "Effect of PVP on the low temperature bonding process using polyol prepared Ag nanoparticle paste for electronic packaging application," Journal of Physics: Conference Series, vol. 379, no. 1, 2012.

[32] Z. Z. Zhang and G. Q. Lu, "Pressure-assisted low-temperature sintering of silver paste as an alternative die-attach solution to solder reflow," IEEE Transactions on Electronics Packaging Manufacturing, vol. 25, no. 4, pp. 279–283, 2002.

[33] T. Morita, E. Ide, Y. Yasuda, A. Hirose, and K. Kobayashi, "Study of Bonding

Technology Using Silver Nanoparticles," Japanese Journal of Applied Physics, vol. 47, no. 8, pp. 6615–6622, 2008.

[34] T. G. Lei, J. N. Calata, G. Lu, X. Chen, and S. Luo, "Low-Temperature Sintering of Nanoscale Silver," Integrated Power Systems (CIPS), 2008 5th International Conference on, vol. 33, no. 1, pp. 98–104, 2010.

[35] Y. Morisada et al., "A low-temperature pressureless bonding process using a trimodal mixture system of Ag nanoparticles," Journal of Electronic Materials, vol. 40, no. 12, pp. 2398–2402, 2011.

[36] G. Zou, J. Yan, F. Mu, A. Wu, J. Ren, and A. Hu, "Low Temperature Bonding of Cu Metal through Sintering of Ag Nanoparticles for High Temperature Electronic Application," The Open Surface Science Journal, vol. 3, no. 1, pp. 70–75, 2010.

[37] H. Nishikawa, X. Liu, X. Wang, A. Fujita, N. Kamada, and M. Saito, "Microscale Ag particle paste for sintered joints in high-power devices," Materials Letters, vol. 161, pp. 231–233, 2015.

[38] H. Zhang, S. Nagao, and K. Suganuma, "Addition of SiC Particles to Ag Die-Attach Paste to Improve High-Temperature Stability; Grain Growth Kinetics of Sintered Porous Ag," Journal of Electronic Materials, vol. 44, no. 10, pp. 3896–3903, 2015.

[39] C. Oh, S. Nagao, and K. Suganuma, "Pressureless Bonding Using Sputtered Ag Thin Films," Journal of Electronic Materials, vol. 43, no. 12, pp. 4406–4412, 2014.

[40] C. Oh, S. Nagao, and K. Suganuma, "Silver stress migration bonding driven by thermomechanical stress with various substrates," Journal of Materials Science: Materials in Electronics, vol. 26, no. 4, pp. 2525–2530, 2015.

[41] C. Oh, S. Nagao, T. Sugahara, and K. Suganuma, "Hillock growth dynamics for Ag stress migration bonding," Materials Letters, vol. 137, pp. 170–173, 2014.

[42] C. Oh, S. Nagao, T. Kunimune, and K. Suganuma, “Pressureless wafer bonding by turning hillocks into abnormal grain growths in Ag films,” Applied Physics Letters, vol. 104, no. 16, 2014.

[43] T. Kunimune, M. Kuramoto, S. Ogawa, T. Sugahara, S. Nagao, and K. Suganuma, “Ultra thermal stability of LED die-attach achieved by pressureless Ag stress-migration bonding at low temperature,” Acta Materialia, vol. 89, pp. 133–140, 2015.

[44] S. Lin et al., “Nano-volcanic Eruption of Silver,” Scientific Reports, vol. 6, p. 34769, 2016.

[45] H. A. Mustain, W. D. Brown, and S. S. Ang, “Transient Liquid Phase Die Attach for High-Temperature Silicon Carbide Power Devices,” IEEE Transactions on Components and Packaging Technologies, vol. 33, no. 3, pp. 563–570, 2010.

[46] P. Snugovsky, P. Arrowsmith, and M. Romansky, “Electroless Ni/immersion Au interconnects: Investigation of black pad in wire bonds and solder joints,” Journal of Electronic Materials, vol. 30, no. 9, pp. 1262–1270, 2001.

[47] E. Seker et al., “The effects of post-fabrication annealing on the mechanical properties of freestanding nanoporous gold structures,” Acta Materialia, vol. 55, no. 14, pp. 4593–4602, 2007.

[48] W. F. Gale and D. A. Butts, “Transient liquid phase bonding,” Science and Technology of Welding and Joining, vol. 9, no. 4, pp. 283–300, 2004.

[49] R. W. Chuang and C. C. Lee, “Silver-indium joints produced at low temperature for high temperature devices,” IEEE Transactions on Components and Packaging Technologies, vol. 25, no. 3, pp. 453–458, 2002.

[50] R. W. Johnson, C. Wang, Y. Liu, and J. D. Scofield, “Power Device Packaging

Technologies for Extreme Environments," IEEE Transactions on Electronics Packaging Manufacturing, vol. 30, no. 3, pp. 182–193, 2007.

[51] P. Hagler, R. W. Johnson, and L. Y. Chen, "SiC die attach metallurgy and processes for applications up to 500°C," IEEE Transactions on Components, Packaging and Manufacturing Technology, vol. 1, no. 4, pp. 630–639, 2011.

[52] K. Chu, Y. Sohn, and C. Moon, "A comparative study of Cn/Sn/Cu and Ni/Sn/Ni solder joints for low temperature stable transient liquid phase bonding," Scripta Materialia, vol. 109, pp. 113–117, 2015.

[53] S. Park, S. Nagao, T. Sugahara, and K. Suganuma, "Mechanical stabilities of ultrasonic Al ribbon bonding on electroless nickel immersion gold finished Cu substrates," Japanese Journal of Applied Physics, vol. 53, no. 4 SPEC. ISSUE, 2014.

[54] S. P. Murarka, "Materials aspects of copper interconnection technology for semiconductor applications," Materials Science and Technology, vol. 17, no. 7, pp. 749–758, 2001.

[55] A. Shah, H. Gaul, M. Schneider-Ramelow, H. Reichl, M. Mayer, and Y. Zhou, "Ultrasonic friction power during AI wire wedge-wedge bonding," Journal of Applied Physics, vol. 106, no. 1, 2009.

[56] S. Park, S. Nagao, T. Sugahara, and K. Suganuma, "Heel crack propagation mechanism of cold-rolled Cu/Al clad ribbon bonding in harsh environment," Journal of Materials Science: Materials in Electronics, vol. 26, no. 9, pp. 7277–7289, 2015.

Chapter 2

Heat-resistant wire interconnection with Ag sinter paste

2.1 Introduction

For the interconnections of high power devices, both copper (Cu) and aluminum (Al) wiring have generally been utilized to form electrical interconnections between semiconductors and circuits on substrates. Cu provides certain advantages such as higher electrical and thermal conductivities for power device interconnection. However, Cu wiring requires special care such as reduction gas, or coatings for bonding due to the formation of Cu oxide under relatively low temperatures [1]. High-purity Al ribbon has already been used in power devices because of its excellent formability in the wiring process. However, high-purity Al has reliability concerns due to its rapid grain coarsening and relatively low current/heat conductivity during high-temperature operation [2]. Electro-migration (EM) is also one of the main risks for Cu and Al under high current [3]. Advanced high-performance wire interconnections are necessary for WBG semiconductors power devices operating under high-temperature and high-current, as these wire interconnections need to survive in severe thermal environments that have not been realized for Si devices.

To ensure the high-performance and reliability of WBG semiconductors power devices, Ag sinter paste has been widely considered as a potential die-attach bonding material due to its high melting point, high electrical conductivity, and its high thermal conductivity compared with conventional soldering materials [4–6]. It has also been reported that sintered Ag nanoparticles film have a longer life expectancy than conventional interconnection materials such as Sn-based solder and Al under high current density [7]. Therefore, it is expected that Ag sinter paste can be used as a wire interconnection material for WBG semiconductor power devices. However, since the power devices consist of various materials such as a semiconductor, a substrate with a metallization layer, and interconnection materials, which have different thermal and mechanical properties, the thermal stress generated by the

mismatch of these properties at high temperature will eventually lead to failure at the interfaces between these materials [8, 9]. Thus, to ensure the performance and reliability of WBG semiconductor power devices, the wire interconnection, and structures including their interfaces must be studied in severe thermal environments.

In this chapter, we evaluated Ag sinter paste wire interconnection (APW) as a novel high-temperature and high-current wire interconnection solution for WBG semiconductor power devices. A wire interconnection using Ag sinter paste between two Cu electrodes coated by Ag was fabricated. The high-temperature reliability including bonding strength and resistivity was evaluated by aging test at 250 ℃ for 1000 h. The high-current reliability was evaluated by EM test with high current 2.2×104 A/cm^2 for 2000 h. Resistance of the wire bonding was evaluated at EM test and microstructure evolution of APW and the joints were characterized by scanning electron microscopy (SEM) with energy-dispersive X-ray spectroscopy (EDS) analysis to confirm influence of EM at the interface between APW and Cu substrate. In addition, to clarify degradation during EM test, electro-thermal–mechanical simulation is then discussed in detail.

2.2 Experimental

2.2.1 Preparation of Ag sinter paste

In this chapter, two kinds of Ag particles were used as starting materials. One was a flake shape having an average particle diameter of 8 μm and a thickness of 260 nm (AgC-239, Fukuda Metal Foil and Powder). The other type of particle was a spherical shape having an average particle diameter of 0.3 μm (FHD, Mitsui Mining and Smelting). These Ag particles were mixed with a weight ratio of 1:1 and further blended with ethylene glycol (10 wt%) to obtain proper printability. This mixture was then blended using a hybrid mixer (HM-500, Keyence) for 10 min.

2.2.2 Preparation of APW for thermal aging test

For APW, the glass substrate was used as a substrate on which to lay Ag sinter paste for maintaining the shape of the wire. The Ag sinter paste was screen-printed onto the glass substrate with dimensions of 2.5 mm × 5 mm × 0.5 mm and placed between two Cu islands on the direct bonded copper (DBC) substrates that have six Cu islands on the both side, as shown in Fig. 2.1a. The mounted specimens were bonded by sintering at 250 °C for 30 min under atmospheric conditions with 0.05 MPa pressure. Prior to the sintering process, the sample was preheated at 180 °C for 5 min to control the evaporation rate of EG and to decrease the tendency to form voids. The surfaces of DBC substrate were metalized with 0.3 μm Ti and 2.0 μm Ag layers via radiofrequency sputtering (Fig. 2.1a). The role of a sputtered Ti layer is to prevent oxidation of Cu, as well as Cu diffusion into the Ag joint during heating [10]. Fig. 2.1b shows that APW was successfully fabricated on the DBC substrates by sintering. Fig 2.1c shows SEM image of surface of APW after sintering, where Ag sinter paste is well sintered featuring microporous structure. Fig. 2.1d shows SEM image of interface

between APW and DBC substrate after the sintering, where Ag sinter paste is well bonded to the DBC with metallization. We performed thermal acceleration tests of thermal aging tests at 250 °C for 1000 h in an oven in air atmosphere, which corresponded to the value applied in the practical WBG power electronic devices.

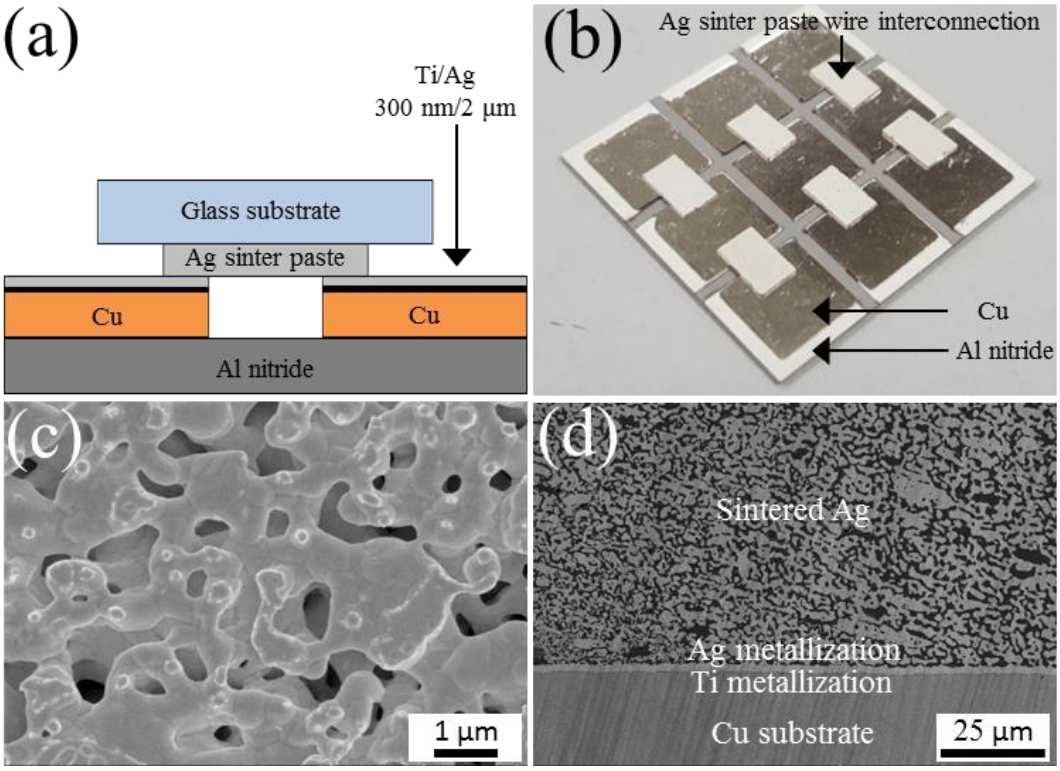

Fig. 2.1 Schematic of APW: (a) Ag-sinter paste is printed on the glass; (b) APW sample for aging test; (c) surface SEM image of APW; and (d) cross-section SEM image of interface between sintered Ag and Cu substrate.

2.2.3 Preparation of APW for EM test

In order to apply high current density, thin and narrow shaped APW were fabricated on the two Cu substrates by the same method for the aging test, as shown in Fig. 2.2a. The APW for EM test had dimensions of 0.5 mm × 10 mm × 0.15 mm. The Cu substrate had dimensions of 4 mm × 10 mm × 0.8 mm that metalized with 0.3 μm Ti and 2.0 μm Ag layers via radiofrequency sputtering. Fig. 2.2b shows EM test setup equipped with power supply and high temperature chamber. The electrical stressing with a current of 17 A was used to evaluate the durability of APW against EM, which corresponds to a current density of around 2.2 × 104 A/cm^2 as accelerated failure condition. Since the porosity of APW can be different depending on the location, the current density (2.2 × 10^4 A/cm^2) was calculated without consideration of porosity due to calculative difficulty including the porosity. Resistance change was monitored by in situ observation under current stressing. The stainless-steel clamps were used at both the ends of the Cu substrates for applying high current. The temperature of APW at the center reached about 270 ℃ due to the Joule heating during EM test, while the temperature at the edge where connected to the substrates was about 250 ℃ due to heat dissipation through the substrates. The temperature was measured by thermocouple wire.

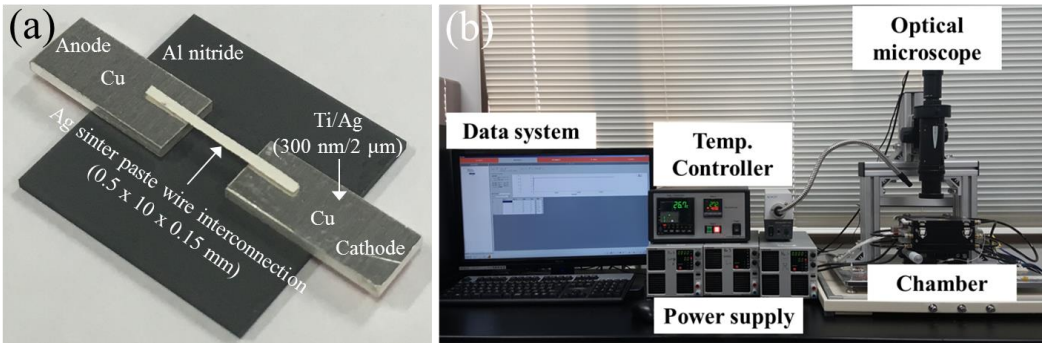

Fig. 2.2 Schematic of EM test: (a) APW sample for EM test; and (b) EM test setup.

2.2.4 Evaluation methods

The electrical resistivity change was measured by a four- point probe analysis with span distance of 2 mm. Source currents were supplied from 500 to 1000 mA. The shear strength of APW joints was evaluated by shear tests (XD- 7500, Dage) at 10 μm/s. The shear position height from the substrate was set to at 10 μm. The cross-sectional microstructure of the APW was observed via field-emission scanning electron microscopy (FE-SEM, SU8020, Hitachi) to verify the wire structure, as well as to observe the interface between APW and Cu substrate for assessing the morphological change after aging and EM test. In addition, EDX (EDAX, Hitachi) analysis was used to observe the influence of EM on the interface between APW and a Cu substrate.

2.2.5 Simulation

Electro–thermal–mechanical simulation [11, 12] was analyzed using finite-element simulation in the EM test specimen. The electro–thermal and thermal–mechanical coupling analyses were performed using commercial software ANSYS 15.0. The electro–thermal analysis provided temperature distribution stemming from Joule heating, which was utilized in thermal–mechanical analysis to calculate the von-Mises stress. The whole structure consisted of Ag paste and Cu substrate without negligible details such as Ti and Ag metallization layer. Thermal, electrical and mechanical parameters used in the simulation are shown in Table 2.1. Natural convection boundary condition was applied to all external surfaces. The heat transfer coefficient was set to about 10 W/m^2K [13], and the ambient temperature was 15 °C. The mechanical boundary conditions can be seen in Fig. 2.3a. The minimum mesh size was used in the simulation to increase analysis accuracy, as shown in Fig. 2.3b.

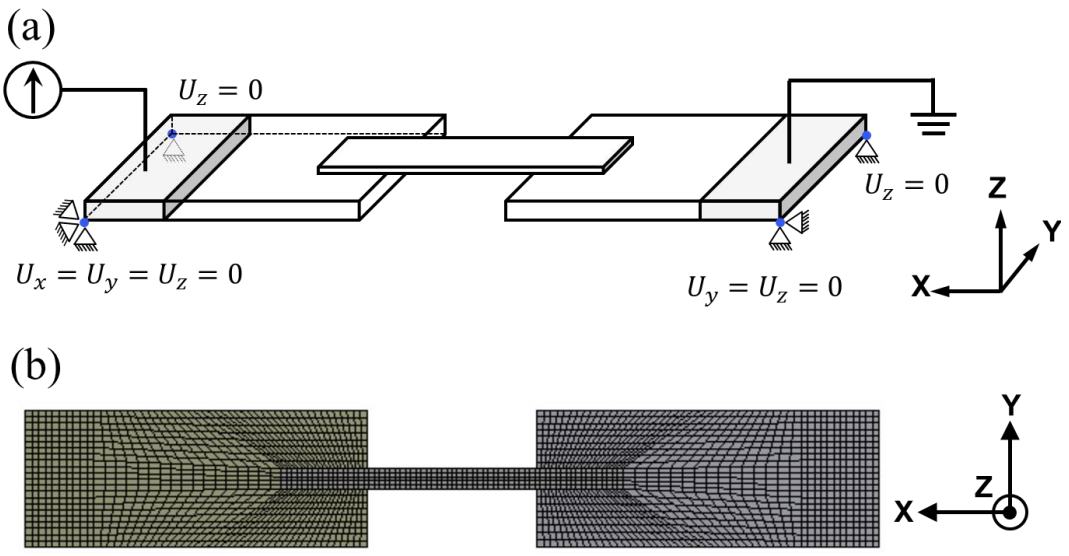

Fig. 2.3 Simulation modeling in ANSYS: (a) The mechanical boundary conditions; and (b) meshed elements.

Table 2.1 Thermal, electrical and mechanical parameters used in the simulation.

properties	Ag paste [4], [9]	Cu substrate
Thermal expansion coefficient (ppm/K)	32.5	16.6
Young's modulus (GPa)	12.9	117
Yield modulus (MPa)	18	150
Tangent modulus (MPa)	6000	518
Poisson's ratio	0.10	0.36
Thermal conductivity (W/m K)	143	120
Specific heat (J/kg K)	235	387
Density (kg/m3)	6300	8300
Resistivity (Ω cm)	4.1×10^{-6}	1.7×10^{-6}

2.3 Results and discussion

2.3.1 Aging test results

2.3.1.1 Resistivity

Fig. 2.4 shows the resistivity change of APW during aging tests in air at 250 °C for 1000 h. At as-sintered state, the resistivity of 4.1×10^{-6} Ω cm was obtained, which is about two times higher than that of conventional wire materials such as Al and Cu [14]. As aging time increased, it was gradually decreased up to 3.4×10^{-6} Ω cm after 1000 h. Fig. 2.5 shows the evolution of microstructure on the APW during aging test. At as-sintered state, a microporous structure was observed with a large number of Ag grains, as shown in Fig. 2.5a. As the aging test proceeded, recrystallization occurred in the sintered Ag network and Ag grains became coarse [15], leading to the thermal coarsening of sintered Ag network by surface diffusion [16], which can be seen as a further sintering process (Fig. 2.5b–d). The porosity of the sintered Ag and average pore size were calculated within a given area of sintered Ag by using imaging software, as shown in Fig. 2.6a, b, respectively. The seven different locations of sintered Ag network were evaluated for calculating means and standard deviation by one-way analysis of variance (ANOVA) and multiple comparison via the Tukey–Kramer test with $P < 0.05$ to indicate significance. The porosity of the sintered Ag decreased with aging time, while the average pore size increased. ANOVA revealed a significant difference in the porosity ($P = 0.0084$). Further analysis using the Tukey–Kramer test showed that the mean porosity for a aging time of 1000 h was significantly higher than that of 0 h ($P = 0.046$), which indicates that the increase of the aging time led to the decreasing of the porosity. In average pore size, ANOVA showed a significant differ- ence ($P = 0.0036$) and Tukey–Kramer test showed that the mean average pore size for a aging time of 1000 h was sig- nificantly higher than that of 0 h ($P = 0.046$). The results indicate that the increase of aging time from 0 to 1000 h led to the

increasing of the pore size. These results agree well with the evolution of microstructure during aging time (Fig. 2.5a–d). The thermal coarsening of sintered Ag network tends to reduce the total surface-to-volume ratio of sintered Ag as well as the total number of pores, forming denser sintered Ag network while increasing pore size during aging test. Thus, both the decreasing of the porosity and further sintering by thermal coarsening were expected to result in an enhancement in resistivity of APW during aging test.

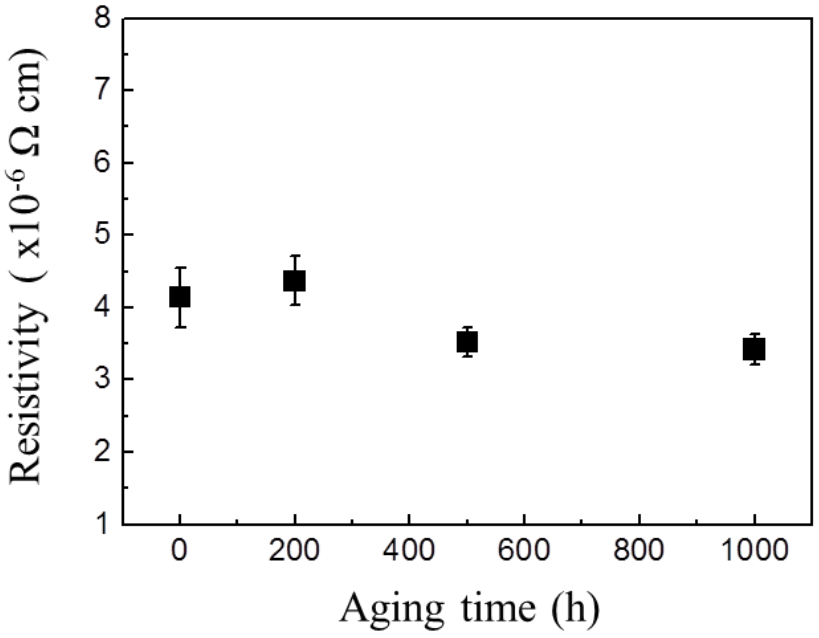

Fig. 2.4 Resistivity change of APW during aging test.

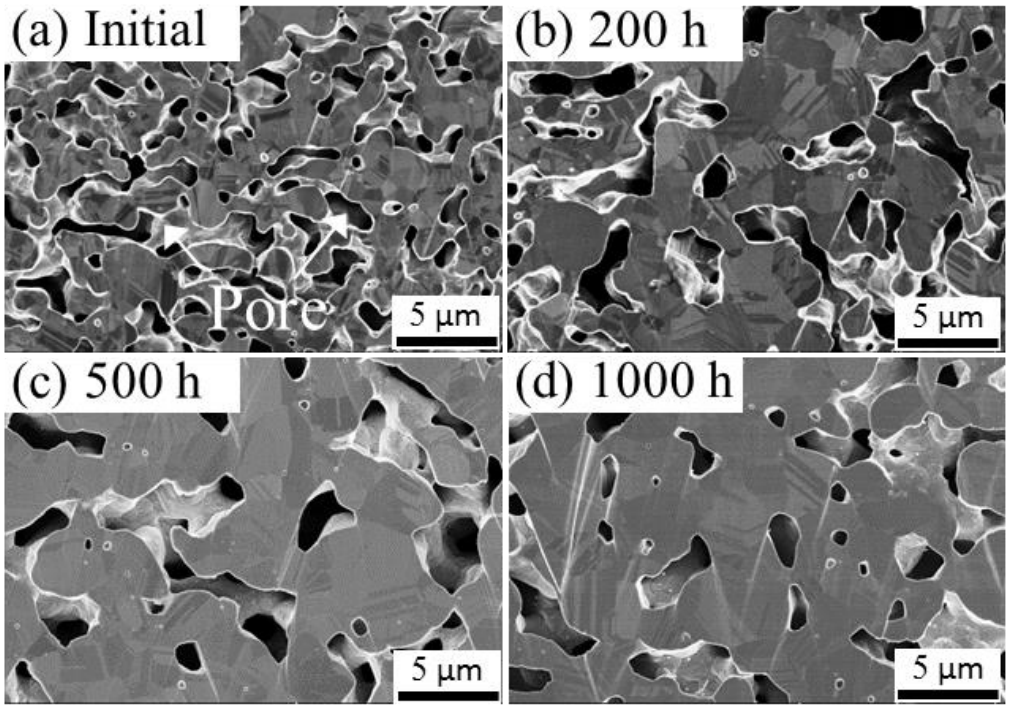

Fig. 2.5 The microstructure evolution of APW during aging test: (a) the as-sintered structure; (b) after aging 200 h; (c) after aging 500 h; and (d) after aging 1000 h.

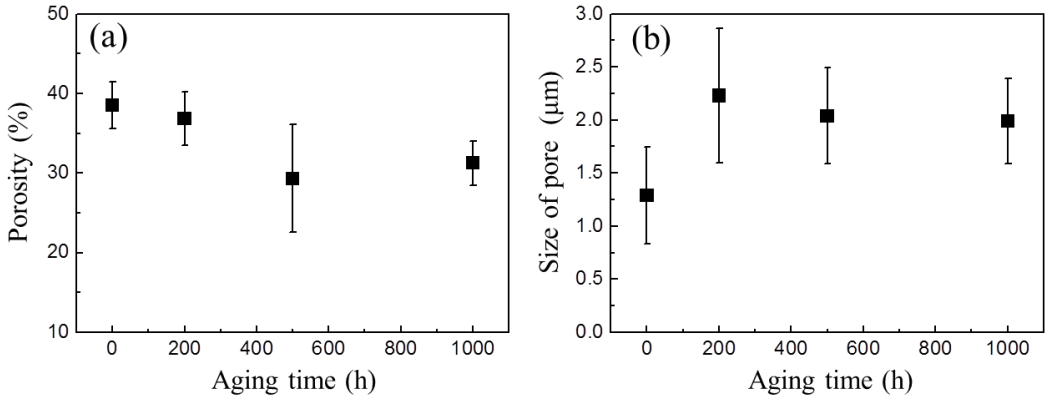

Fig. 2.6 The evolution of APW during aging test: (a) the porosity change; and (b) the size of pore change.

2.3.1.2 Shear strength

The mechanical strengths of the APW were compared to those of Al ribbon interconnection which is generally used in high power electronic devices. The Al ribbons were fabricated on electroless nickel immersion gold (ENIG) finished DBC substrate by ultrasonic sound bonding. Fig. 2.7 shows the shear strength of joints in the APW and Al ribbon interconnection after aging tests at 250 °C. The schematic views were shown in Fig. 2.7. The error bar was calculated from the standard deviation of 5 specimens. The scattering in the shear strength is likely from the non-uniform contacts between the samples, which is caused by the thermal warpage of a Cu substrate. In the APW, the initial shear strength was 17 MPa, which, while high enough, was maintained even after an aging test of 1000 h. However, in the Al ribbon interconnection, the degradation of shear strength was observed during aging due to the formation of brittle intermetallic phases [17] or interface corrosion [18], leading to a crack or interface failure [19]. In the present work, no degradation was observed in shear strength of the APW during aging test. It is supposed that the above-mentioned degradation at the interface was prevented by the use of the same materials in wire and metallization layer.

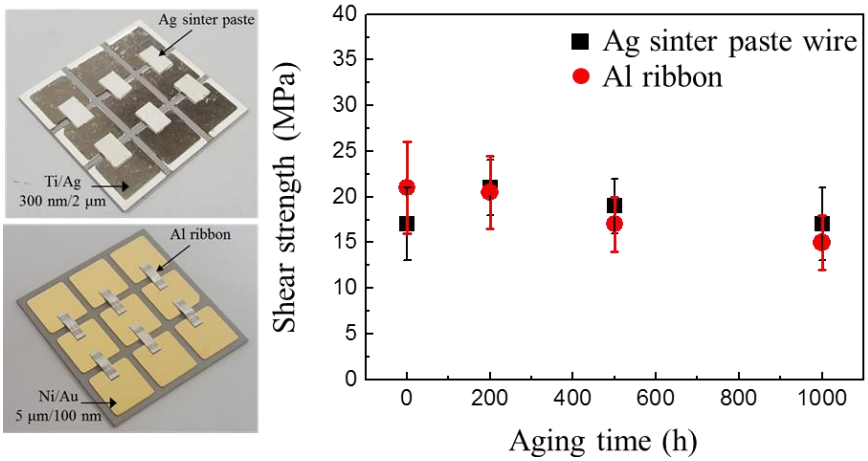

Fig. 2.7 Shear strength of the APW and Al ribbon during aging test.

2.3.1.3 Evolution of microstructure

Fig. 2.8 shows the microstructure evolution of APW at the interface during aging test. The initial APW was well bonded to the DBC substrate, as shown Fig. 2.8a. With increasing aging time, the interfacial degradation such as interface corrosion and crack was not observed between the APW and the DBC substrate, as shown Fig. 2.8b–d. However, voids formed in the Ag metallization layer after aging test for 500 h, as shown in Fig. 8c, and more appeared with increased aging time (Fig. 2.8d). The reason for formation of voids in the Ag metallization layer is a dewetting phenomenon [20]. It was reported that Ag atoms in the Ag metallization layer were passively absorbed into the porous Ag joint to support the growth of the Ag network, leading to void formation in the Ag metallization when coarsening is continuously triggered at 250 °C. In the present work, the shear strength did not change even after aging 1000 h, indicating that the voids did not influence the shear strength. This can be explained that initial interface connection ratio between sintered Ag and metallization layer did not change compared with that after aging test for 1000 h, although voids appeared in the Ag metallization layer [21]. Thus, the APW is able to maintain a strong joint during aging test.

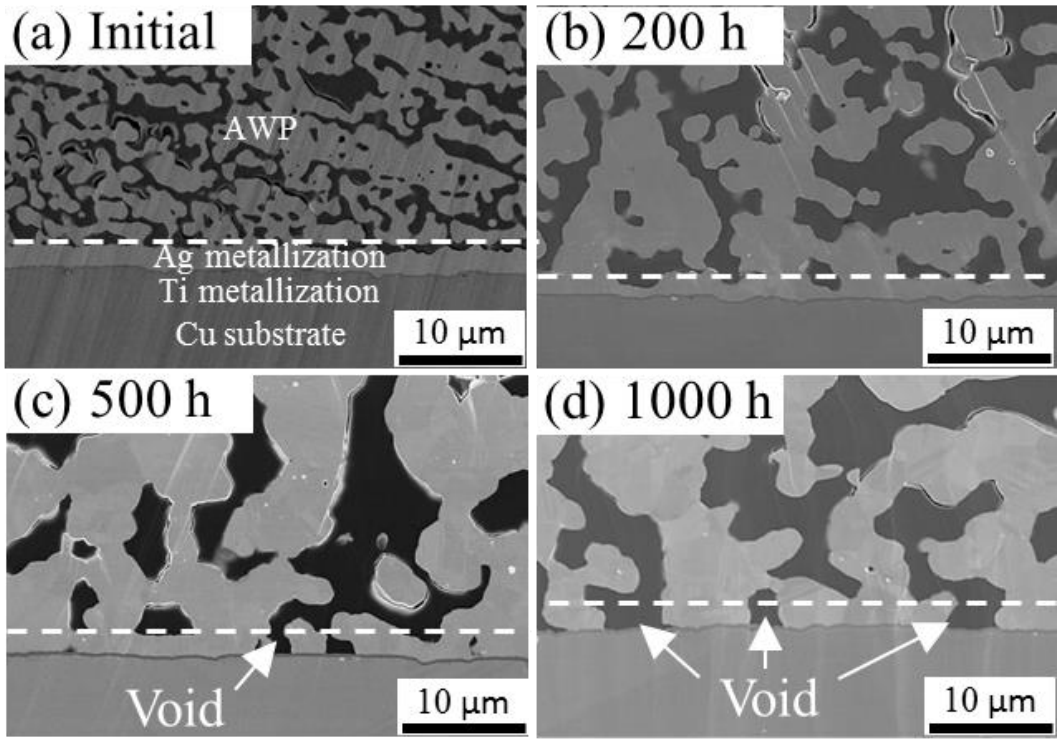

Fig. 2.8 The microstructure evolution of APW at the interface during aging test: (a) the as-sintered structure; (b) after aging 200 h; (c) after aging 500 h; and (d) after aging 1000 h.

2.3.2 Electromigration test results

2.3.2.1 Resistance

The accelerated condition of current density was about 2.2 × 104 A/cm^2. A temperature of 250–270 °C was obtained by Joule heating during EM test, which is the expected temperature for the practical WBG power electronic devices [4]. In order to certify durability of APW including wire and interfaces, resistance changes were evaluated as a function of time for two samples during EM test, as shown in Fig. 2.9. The resistance of APW did not change significantly up to 1000 h and then only slightly increased up to 2000 h. This slight change is more stable than conventional wire interconnection material such as Al and Cu under high temperature and high current density [22, 23].

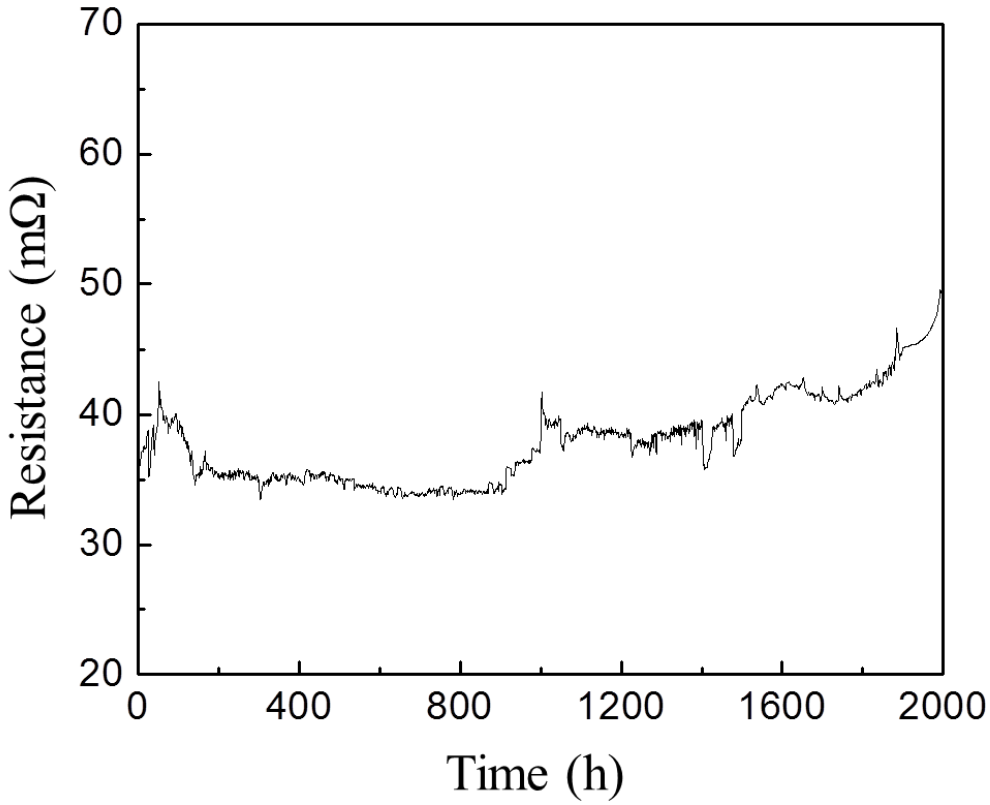

Fig. 2.9 Resistance change of APW during EM test.

2.3.2.2 Shear strength

Fig. 2.10 shows the shear strength of joints in the APW at the anode and cathode side after EM tests. The error bar was calculated from the standard deviation of 2 specimens. The shear strength decreased at the anode side, and more decreased at the cathode side with increased EM time. As mentioned earlier in "2.3.1 aging test results", no degradation was observed in shear strength during aging test (Fig. 2.5) because interfacial degradations were prevented by the use of the same materials in wire and metallization layer. On the other hand, the degradation of shear strength was observed during EM test. These results indicate that during EM test, the joint suffered from electro–thermal stresses under high current density, which causes more significant effects and severer damages compared with aging test.

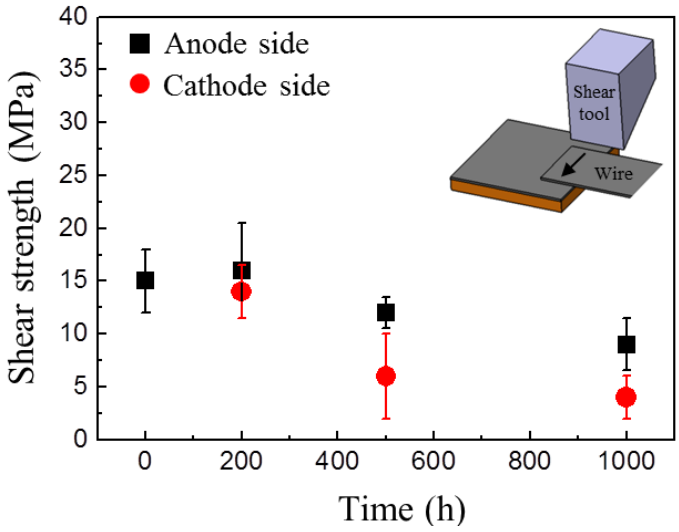

Fig. 2.10 Shear strength of APW during EM test.

2.3.2.3 Evolution of microstructure

To clarify the mechanism of EM failure for APW, microstructure evolution was observed during EM test. Fig. 2.11 shows the sequential cross-sectional SEM images of the interface between APW and Cu substrate on both anode and cathode sides after EM tests for 0, 500 and 1000 h. As shown in Fig. 2.10a, b, the initial APW has a microporous structure featuring a large number of Ag grains. As the EM test proceeds, the coarsening of Ag network occurred due to Joule heating on both anode and cathode sides (Fig. 2.11c, d). However, when the EM test time increased to 1000 h, cracks were observed both at the interface and within the sintered microstructure near the end of the joint on the cathode side, as shown in Fig. 2.11f, while Fig. 2.11e shows robust sintered Ag structure on the anode side.

Fig. 2.12 shows magnified views of the interface between APW and Cu substrate corresponding to Fig. 2.11. In the case of the anode side, Ag and tiny voids were observed inside Cu substrate with increasing EM test time (Fig. 2.12c), and grew subsequently after EM test for 1000 h, as shown in Fig. 2.12e. This was verified by EDX mapping corresponding to Fig. 2.12e, as shown in Fig. 2.13a. SEM/EDX results indicate that Ag atoms had migrated from APW to Cu substrate by electric current stressing along the direction of electron flux (from cathode to anode) [24], resulting in void formation inside APW and the migration of Ag atoms into Cu substrate. Because of migration of Ag atoms into Cu substrate, compressive stress induced by EM should occur at the interface between APW and Cu substrate from the direction of APW. On the other hand, it was also found that Cu moved into APW layer as shown in Fig. 2.13a. Different from the Ag atoms migrating into Cu substrate, the Cu atoms migration into APW was induced by the diffusion of Cu atoms at high temperature (250 °C) at the interface during the EM test. Since the migrated Ag consumed the space occupied by Cu atoms, large plastic stresses were generated at the interface between Ag and Cu due to

significant differences in mechanical properties and volume. Therefore, voids nucleated around Ag, migrated into the Cu substrate, and grew due to the stress when EM of Ag into Cu substrate occurs. In addition, Cu oxide was also observed in the APW (Fig. 2.12c, e), which means Cu penetrated through the voids or cracks in the Ti barrier layer and formed an Cu oxide inside the APW during EM test due to the high temperature caused by Joule heating [8]. The source of oxygen was conjectured to be residual oxygen in the APW. As for the cathode side, Cu oxide appeared inside APW while voids formed inside Cu substrate after EM test for 500 h, as shown in Fig. 2.12d. When the EM test time increased to 1000 h, cracks formed inside Cu substrate while Cu oxide became coarse (Fig. 2.12f). This was verified by EDX mapping corresponding to Fig. 2.12f, as shown in Fig. 2.13b. In this case, since the Cu atoms had migrated from Cu substrate to APW by electric current stressing along the direction of electron flux, the direction of compressive stress induced by EM was opposite in the case of anode. In addition, because the Cu atoms moved into APW induced by high temperature diffusion, Cu atoms migrated very rapidly into APW, leading to void formation at the surface of Cu substrate. With increased EM test time, cracks formed inside Cu substrate caused by continuous void formation and brittleness of Cu oxide, which is believed a main reason for increased resistance in APW during EM test.

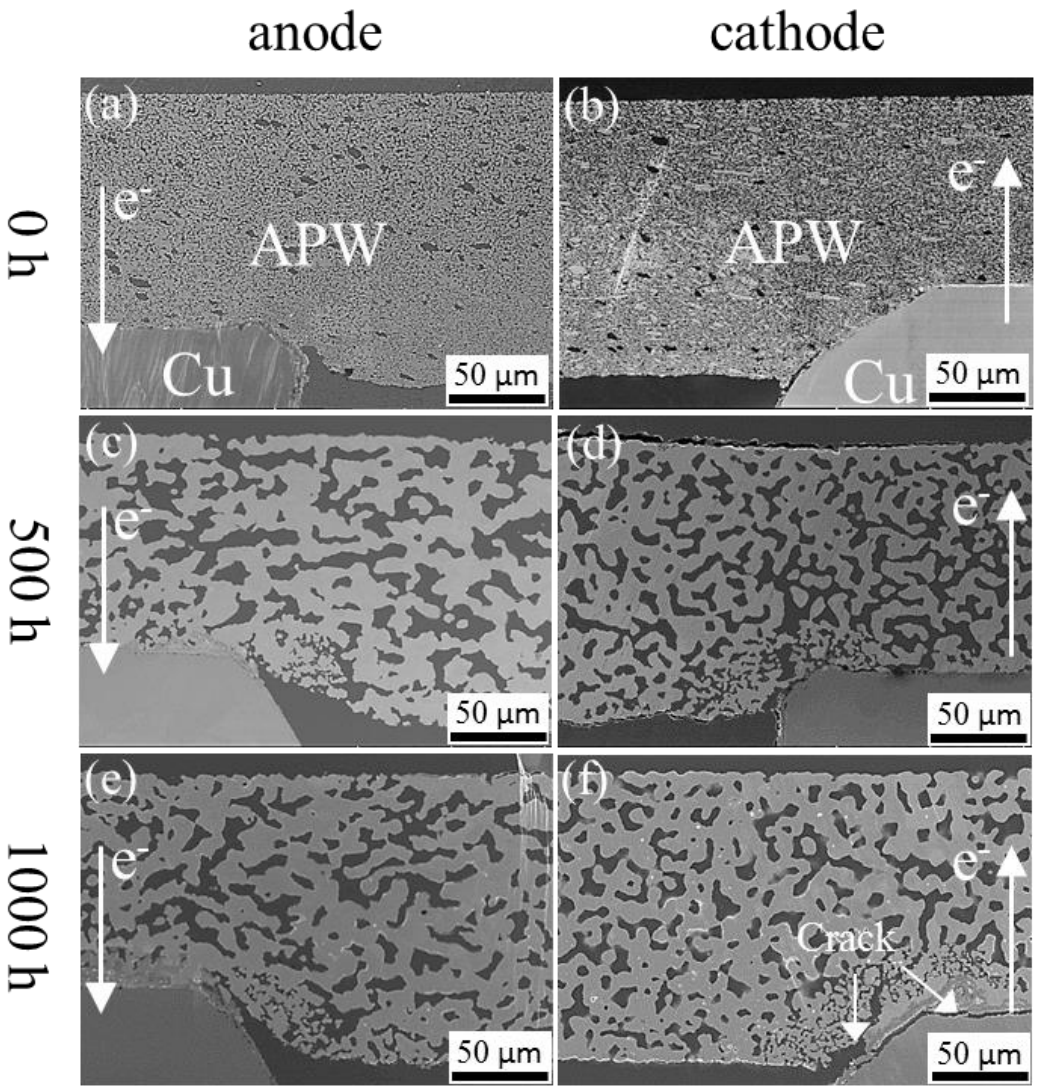

Fig. 2.11 The microstructure evolution of APW during EM test: anode side (a) the as-sintered structure; (b) after test 500 h; (c) after test 1000 h, and cathode side (a) the as-sintered structure; (b) after test 500 h; (c) after test 1000 h.

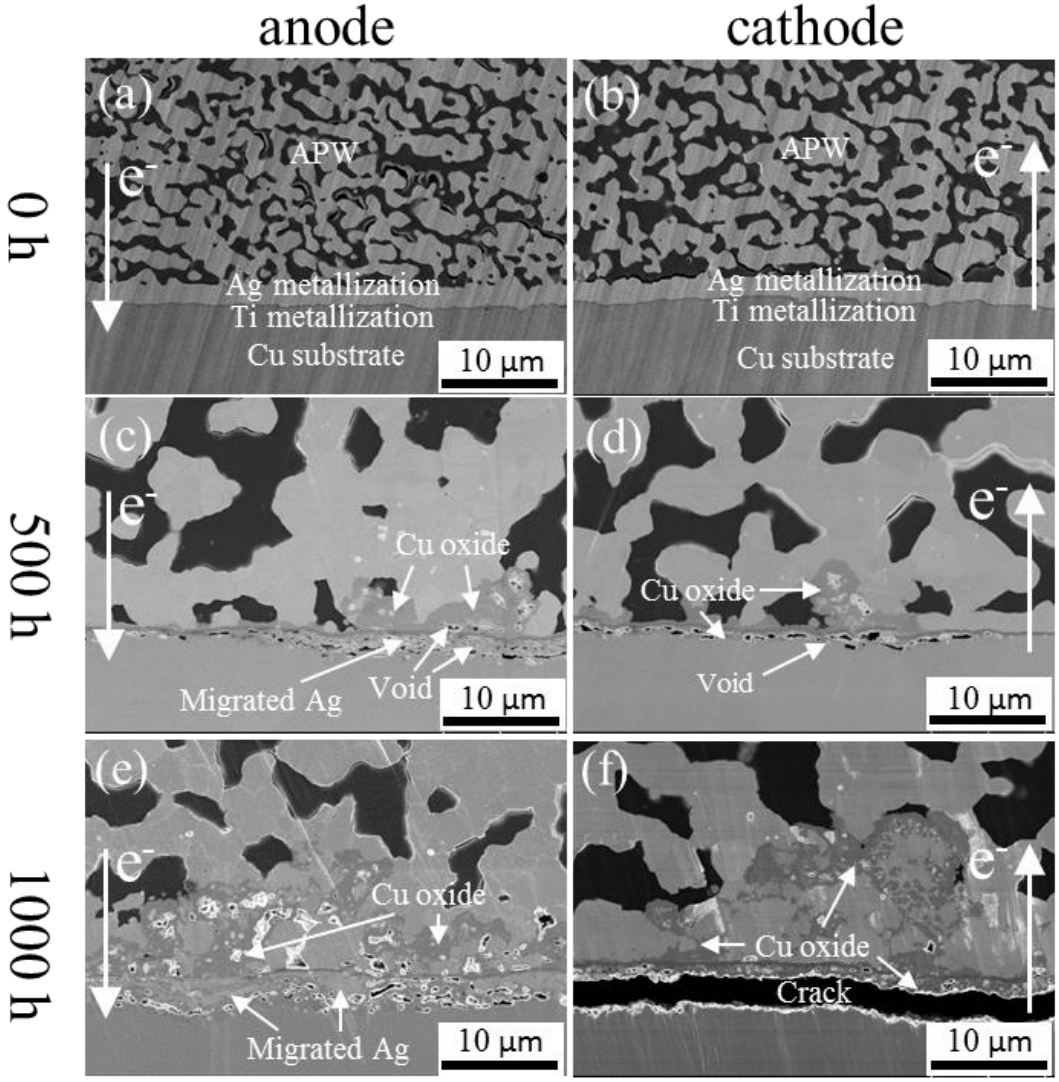

Fig. 2.12 Magnified views of the interface corresponding to Fig .7: anode side (a) the as-sintered structure; (b) after test 500 h; (c) after test 1000 h, and cathode side (a) the as-sintered structure; (b) after test 500 h; (c) after test 1000 h.

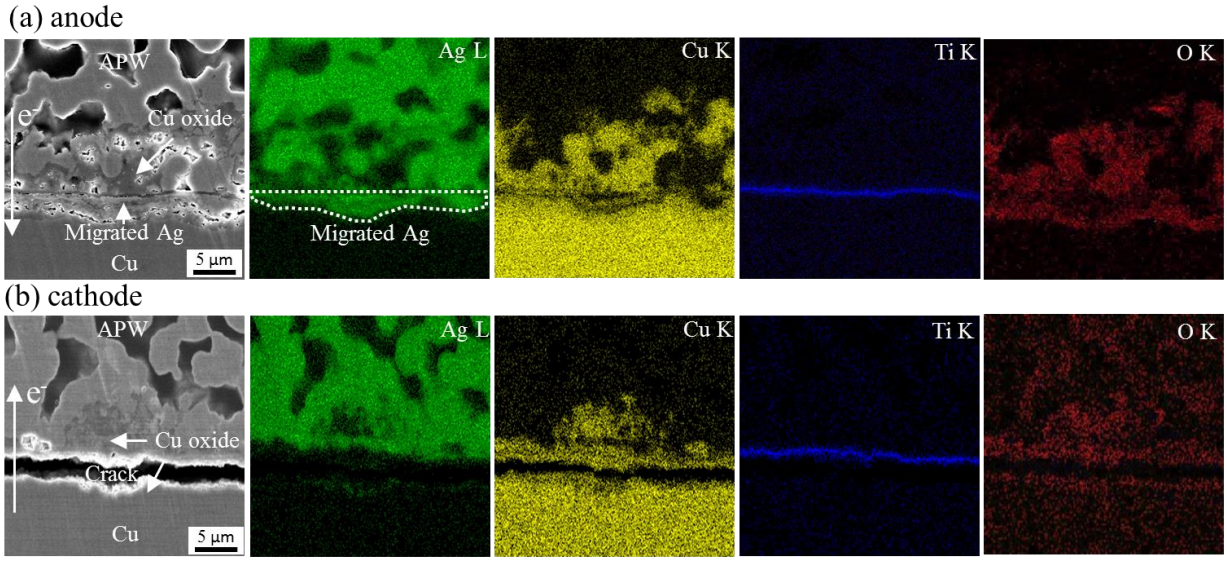

Fig. 2.13 EDS images of interface between sintered Ag and metallization layer after EM test for 1000 h: (a) anode side; (b) cathode side.

2.3.2.4 Simulation verification

As shown in Figs. 2.11 and 12, EM and cracks occurred during EM test near the end of joint both at anode and cathode sides. To clarify the cause of these behaviors, electro–thermal–mechanical simulation was analyzed by using a three dimensional (3D) finite element model analysis, as shown in Fig. 2.14. The maximum current density was observed near the end of joints, which was 50% higher than those of other position in APW, as shown in Fig. 2.14a. Meanwhile, generated temperature near the end of joints caused by Joule heating obtained about 290 °C (Fig. 2.14b), which was about 40 °C higher than measured temperature by thermocouple. It is inferred that the difference between simulated and measured temperature is likely from a lack of thermal properties depending on the temperature. Fig. 2.14c shows the von–misses stress distribution, which was caused by CTE mismatch between APW and Cu substrate. The maximum stress appeared at the same position (Fig. 2.14a) as the maximum current density, as shown in Fig. 2.14c. The results indicate that initial EM mainly occurred at the location of maximum current density due to the higher driving force to migrate atoms, and subsequently, the von-misses stress accumulated at the same position as maximum current density, implying that the crack induced by the shear stress might begin and propagate from the edge to center (Fig. 2.11f).

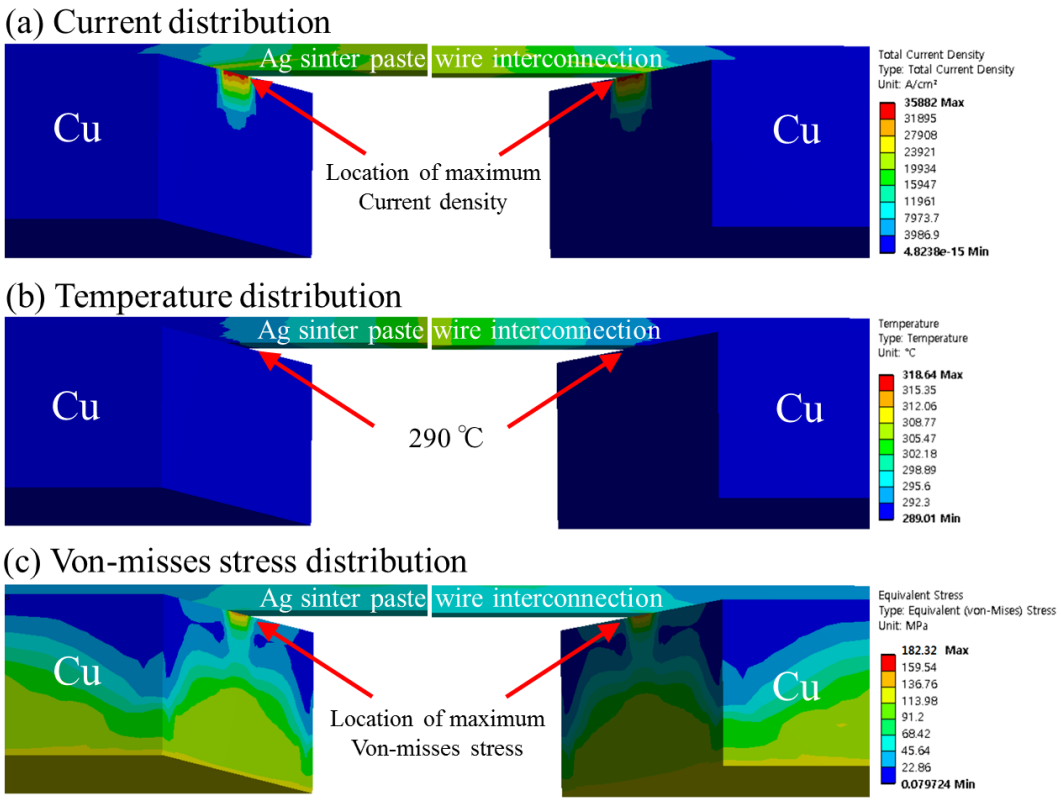

Fig. 2.14 FE simulation results: (a) current density distribution; (b) temperature distribution; and c von-misses stress distribution.

2.4 Conclusions

In this chapter, we explored the possibility of using Ag sinter paste as a novel wire bonding solution for alternative interconnection material of WBG semiconductor devices. The high-temperature reliability and the high-current reliability were evaluated by aging test at 250 °C for 1000 h and by EM test at 2.2 × 104 A/cm^2 for 2000 h. The new findings of this study can be summarized as follows:

1. The resistivity of about 4.1 × 10^{-6} Ω cm was obtained and enhanced up to 3.4 × 10^{-6} Ω after aging for 1000 h by coarsening of sintered Ag network.
2. Serious reliability problems at high temperatures such as brittle intermetallic phases or interface corrosion which is the main failure mechanism in conventional wire bonding were prevented by the use of the same materials in wire and metallization layer, leading to excellent heat-resistance at even 250 °C
3. Resistivity of APW did not rise significantly up to roughly 1000 h and thereafter only slightly increased with EM test time. This slight change is considerably more stable than that of conventional Al wire bonding at high temperature and high current density.
4. The initial EM mainly occurred near the end of joint between the APW and Cu substrate, which is the location of maximum current density, and subsequently, the von-misses stress accumulated by Joule heating near at the same position as maximum current density, implying that the crack induced by the shear stress might begin and propagate from the edge to center.

References

[1] H. Xu, I. Qin, H. Clauberg, B. Chylak, and V. L. Acoff, “Behavior of palladium and its impact on intermetallic growth in palladium-coated Cu wire bonding,” Acta Materialia, vol. 61, no. 1, pp. 79–88, 2013.

[2] M. Schneider-Ramelow and C. Ehrhardt, “The reliability of wire bonding using Ag and Al,” Microelectronics Reliability, vol. 63, pp. 336–341, 2016.

[3] J. R. Black, “Electromigration failure modes in aluminum metallization for semiconductor devices,” Proceedings of the IEEE, vol. 57, no. 9, pp. 1587–1594, 1969.

[4] K. Suganuma, S. Sakamoto, N. Kagami, D. Wakuda, K. S. Kim, and M. Nogi, “Low-temperature low-pressure die attach with hybrid silver particle paste,” Microelectronics Reliability, vol. 52, no. 2, pp. 375–380, 2012.

[5] P. Peng, A. Hu, A. P. Gerlich, G. Zou, L. Liu, and Y. N. Zhou, “Joining of Silver Nanomaterials at Low Temperatures: Processes, Properties, and Applications,” ACS Applied Materials and Interfaces, vol. 7, no. 23, pp. 12597–12618, 2015.

[6] R. Khazaka, L. Mendizabal, and D. Henry, “Review on joint shear strength of nano-silver paste and its long-term high temperature reliability,” Journal of Electronic Materials, vol. 43, no. 7, pp. 2459–2466, 2014.

[7] J. N. Calata, G. Q. Lu, K. Ngo, and L. Nguyen, “Electromigration in sintered nanoscale silver films at elevated temperature,” Journal of Electronic Materials, vol. 43, no. 1, pp. 109–116, 2014.

[8] C. Pei, C. Chen, K. Suganuma, and G. Fu, “Thermal Stability of Silver Paste Sintering on Coated Copper and Aluminum Substrates,” Journal of Electronic Materials, vol. 47, no. 1, pp. 811–819, 2018.

[9] C. Chen, S. Nagao, H. Zhang et al., "Mechanical Deformation of Sintered Porous Ag Die Attach at High Temperature and Its Size Effect for Wide-Bandgap Power Device Design," Journal of Electronic Materials, vol. 46, no. 3, pp. 1576–1586, 2017.

[10] H. Zhang, C. Chen, S. Nagao, and K. Suganuma, "Thermal Fatigue Behavior of Silicon-Carbide-Doped Silver Microflake Sinter Joints for Die Attachment in Silicon/Silicon Carbide Power Devices," Journal of Electronic Materials, pp. 1–6, 2016.

[11] J. P. Yang, G. K. Lau, C. P. Tan, N. B. Chong, B. Thubthimthong, and Z. M. He, "An electro-thermal micro-actuator based on polymer composite for application to dual-stage positioning systems of hard disk drives," Sensors and Actuators, A: Physical, vol. 187, pp. 98–104, 2012.

[12] N. Mitchell, "Two-way interaction between the strand voltage-current characteristic and the overall conductor behaviour in cabled low temperature superconductors," Physica C: Superconductivity and its Applications, vol. 401, no. 1–4, pp. 28–39, 2004.

[13] X. Zhu, H. Kotadia, S. Xu et al., "Electromigration in Sn-Ag solder thin films under high current density," Thin Solid Films, vol. 565, pp. 193–201, 2014.

[14] S. Park, S. Nagao, T. Sugahara, and K. Suganuma, "Mechanical stabilities of ultrasonic Al ribbon bonding on electroless nickel immersion gold finished Cu substrates," Japanese Journal of Applied Physics, vol. 53, no. 4 SPEC. ISSUE, 2014.

[15] J. E. Bailey, "Electron microscope observations on the annealing processes occurring in cold-worked silver," Philosophical Magazine, vol. 5, no. 56, pp. 833–842, 1960.

[16] M. Hakamada and M. Mabuchi, "Thermal coarsening of nanoporous gold: Melting or recrystallization," Journal of Materials Research, vol. 24, no. 2, pp. 301–304, 2009.

[17] H. Xu, C. Liu, V.V. Silberschmidt et al., "Behavior of aluminum oxide, intermetallics

and voids in Cu-Al wire bonds," Acta Materialia, vol. 59, no. 14, pp. 5661–5673, 2011.

[18] M.R. Choi, H.G. Kim, T.W. Lee et al., "Microstructural evaluation and failure analysis of Ag wire bonded to Al pads," Microelectronics Reliability, vol. 55, no. 11, pp. 2306–2315, 2015.

[19] R. K. Burla, L. Chen, C. A. Zorman, and M. Mehregany, "Development of nickel wire bonding for high-temperature packaging of SiC devices," IEEE Transactions on Advanced Packaging, vol. 32, no. 2, pp. 564–574, 2009.

[20] H. Zhang, S. Nagao, K. Suganuma, H. J. Albrecht, and K. Wilke, "Thermostable Ag die-attach structure for high-temperature power devices," Journal of Materials Science: Materials in Electronics, vol. 27, no. 2, pp. 1337–1344, 2016.

[21] C. Chen, K. Suganuma, T. Iwashige, K. Sugiura, and K. Tsuruta, "High-temperature reliability of sintered microporous Ag on electroplated Ag, Au, and sputtered Ag metallization substrates," Journal of Materials Science: Materials in Electronics, vol. 29, no. 3, pp. 1785–1797, 2018.

[22] C.K. Hu, D. Canaperi, S.T. Chen et al., "Electromigration Cu mass flow in Cu interconnections," Thin Solid Films, vol. 504, no. 1–2, pp. 274–278, 2006.

[23] A. Witvrouw, H. Bender, P. Roussel, and K. Maex, "Modeling and microstructural characterization of incubation, time-dependent drift and saturation during electromigration in Al-Si-Cu stripes," Microelectronics Reliability, vol. 39, no. 11, pp. 1603–1616, 1999.

[24] K.-C. Chen, W.-W. Wu, C.-N. Liao, L.-J. Chen, and K. N. Tu, "Observation of atomic diffusion at twin-modified grain boundaries in copper," Science, vol. 321, no. 5892, pp. 1066–1069, 2008.

Chapter 3

Heat-resistant die-attach with cold-rolled Ag sheet

3.1 Introduction

As mentioned in *Section 1.2.1*, Ag sinter paste as a die-attach material is generally used to ensure the high performance and reliability of WBG power devices operating at high temperatures. However, Ag sinter paste has many issues to be resolved before mass production, especially the complex processes of Ag particle synthesis and the suitable fabrication of Ag paste for the bonding process. Additionally, the Ag paste changes into a microporous structure after sintering under a limited applied pressure [1–3]. Such a microporous structure can decrease the electrical and thermal conductivities, depending on the porosity. The joint strength is also affected by the microporous structure [4]. On the other hand, metal sheet preforms are widely used to facilitate die attach [5–7]. They provide better uniform contact over entire bonding areas compared with sinter paste, which requires an organic solvent [8]. Sheet preforms have been also studied as a stress buffer for releasing stress caused by the coefficient of thermal expansion (CTE) mismatch between the chip and substrate [9–11].

In addition, it has been reported that hillocks can appear on surfaces of metallic films under compressive stress caused by the CTE mismatch between films and substrates [12–14]. Previous research revealed that the growth of hillocks on Ag thin films can promote interface bonding in the die-attach structure [15–20], which is referred to as stress migration bonding (SMB). The mechanism of SMB was also investigated with "nano-volcanic eruption" theory as mentioned in *Section 1.2.2*. Thus, it is expected that two Ag-coated surfaces can be bonded together by using a bulk Ag sheet if dense hillock growth can be induced by optimizing the microstructure and stress condition inside the sheet properly. In this case, because the Ag sheet has excellent thermal, electrical, and mechanical properties even compared with a sintered microporous Ag layer, it can be extremely advantageous to use an optimized Ag sheet

as a replacement for a microporous sintered Ag for high-power devices.

In this chapter, a bonding technology with a cold-rolled Ag sheet is explored for fabricating a die-attach structure based on SMB. Hillock and whisker growth were commonly observed on the coated metallic films on the Si or metal substrate because of the stress-migration induced by the CTE mismatch. However, in the case of a metal sheet, hillock growth is rarely reported, because of the lack of driving force for stress migration. Here, we optimized the hillock growth on the Ag sheet by cold-rolling to realize interface bonding between the sheet and sputtered films. Heavy deformation induced by cold-rolling is utilized as a driving force for stress migration, and dense Ag hillock growth can be formed on the cold-rolled Ag sheet by simple heat treatment in air. In addition, the bonding interface was observed via transmission electron microscopy (TEM) to confirm the bonding mechanism between two faces.

3.2 Experimental

3.2.1 Materials and bonding process

Commercial high-purity Ag sheets (99.99 wt %) with a length and width of 50.0 and 4.0 mm, respectively, were used as bonding sheets. The initial thickness of the Ag sheets varied 0.1, 0.3, 0.5, and 1.0 mm. The Ag sheets were annealed at 400 °C for 1 h to achieve a uniform grain size. Cold rolling was applied in this study to obtain grain refinement and compressive residual stress, which are critical factors for hillock formation [14, 16]. The Ag sheets with a thickness of 0.3, 0.5 and 1 mm were cold-rolled up to 0.1 mm, which corresponds to reduction ratio of 66, 80 and 90%, respectively. The cold rolling was performed in multiple rolling passes; a thickness reduction of 0.10 mm per pass at room temperature was achieved with a rolling speed of 0.04 m s−1, without lubrication, as shown in Fig. 3.1a. After the rolling, the Ag sheets were cut into 4.0 × 4.0 mm^2 pieces. A 4.0 × 4.0 mm^2 Si chip and 8 × 16 mm^2 Cu substrates were metalized with 0.1 μm Ti and 1.0 μm Ag layers via radiofrequency sputtering. A sputtered Ti layer prevents surface oxidation of Cu as well as diffusion of Cu from the substrate. After cleaning all the substrates and cold-rolled Ag sheets via ultrasonication in acetone for 5 min, a Ag sheet was sandwiched between them, as shown in Fig. 3.1b. The samples were placed on a hot plate under a load of 1 MPa and heated in air for 1 h, as shown in Fig. 3.1c. The optimum bonding conditions for the die-attach structure were obtained in the temperature range of 250 to 400 °C.

3.2.2 Characterization methods

The cross-sectional microstructure of the joints was observed via field-emission scanning electron microscopy (SEM; Hitachi SU8020) to verify the bonding structure at the interface, as well as the surface of the samples for assessing the morphological change after heating. Via

this process, two substances were successfully bonded. Fig. 3.1d shows an example SEM image after the bonding at 300 °C, where the Ag sheet is well-bonded to the Ag thin film on both the Si dummy chip and the Cu substrate. Electron backscatter diffraction (EBSD; Oxford Instruments) was used to reveal the microstructure change in the Ag sheet after cold-rolling. The die shear strength of the joints was measured via die-shear tests (DAGE XD-7500) at a shear rate of 50 μm s^{-1}. The change of the residual stress in the Ag sheet after cold-rolling was determined via X-ray stress measurements (Pulstec U-360) using the cos α method [21–23]. The shear position height from the substrate surface was set as 100 μm. Seven bonded specimens were tested to obtain one dataset. All the results were analyzed using a one-way analysis of variance (ANOVA) and multiple comparison via the Tukey–Kramer test with $p < 0.05$ to indicate significance. TEM (JEM-ARM200F, JEOL) were performed on interfacial cross-sections to determine the influence of hillock formation on the interface bonding quality.

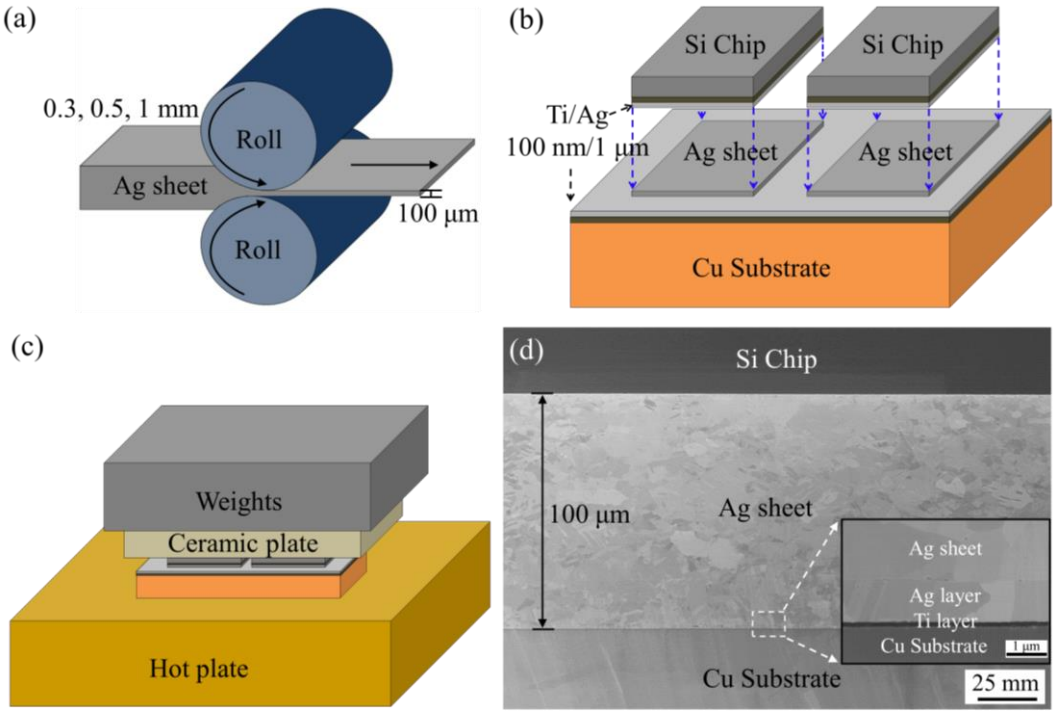

Fig. 3.1 Schematic of the bonding process. The Ag sheet is cold-rolled to 90% thickness reduction (a); Ag sheet sandwiched between the coated Si dummy chip and the Cu substrate (b); the mounted specimens placed on a hot plate for heating; (c) and cross-sectional SEM image of SMB using a cold- rolled Ag sheet bonded at 300°C under an applied pressure of 1MPa (d).

3.3 Results and discussion

3.3.1 Mechanism for hillock formation

The Hillock growth on the cold-rolled Ag sheet and sputtered Ag thin films was observed. Fig. 3.2a shows an SEM image of the surfaces of the Ag sheet cold-rolled to 90% thickness reduction and sputtered Ag thin films on the Si chip and Cu substrate. Sub-microsize fine grains appeared on the surface of the cold-rolled Ag sheet, which were similar to the grains in the as-deposited Ag thin films prepared using a sputtering system. After heating at 250 ℃, hillock growth was observed on the surfaces of the Ag sheet and sputtered Ag thin film, as shown in Fig. 3.2b. The formation of Ag hillocks in sputtered Ag film has been attributed to stress migration induced by thermal stress or residual stresses [15–19]. In this mechanism, the hillock growth for the Ag thin film is caused by a specific reaction between Ag and O called "nano-volcanic eruption". The migration phenomenon of Ag–O fluids towards the surface through grain boundaries plays a key role in hillock formation [20].

In the case of the cold-rolled Ag sheet, many hillocks were detected on the surface without thermal stress caused by CTE mismatch. The hillock growth on the Ag sheet is attributed to the heavy deformation induced by cold rolling, which resulted in grain refinement and compressive residual stress. We measured the change of the residual stress in the Ag sheet after cold-rolling to verify the influence of compressive stress for hillock formation. Before the cold-rolling, a residual stress of 14 MPa was measured in the tensile direction, whereas this became a compressive stress of −51 MPa after the cold-rolling. It was reported that the direction of the generated residual stress was opposite to the deformation direction [24]. Therefore, compressive stress may induced by the large deformation of the Ag sheet during the cold-rolling process. In addition, the microstructure change of the Ag sheet after the cold-rolling was investigated using EBSD maps, as shown Fig. 3.3. After the cold

rolling, the grain size of the Ag sheet had decreased from the microscale to the sub-microscale, leading to the density increase of the grain boundary, which provided a pathway to migrate Ag atoms for hillock formation. Hillock formation of the cold-rolled Ag sheet can be driven by relaxation of compressive residual stress through the increase of the density of the grain boundary during the cold-rolling process. In addition, it was reported that the compressive stress on the sputtered Ag/Si substrate structure was approximately −150 MPa [16], which is larger than that on the cold-rolled Ag sheet. Therefore, compared with the cold-rolled Ag sheet, larger hillocks were formed on the sputtered Ag/Si substrate structure (Fig. 2.2b).

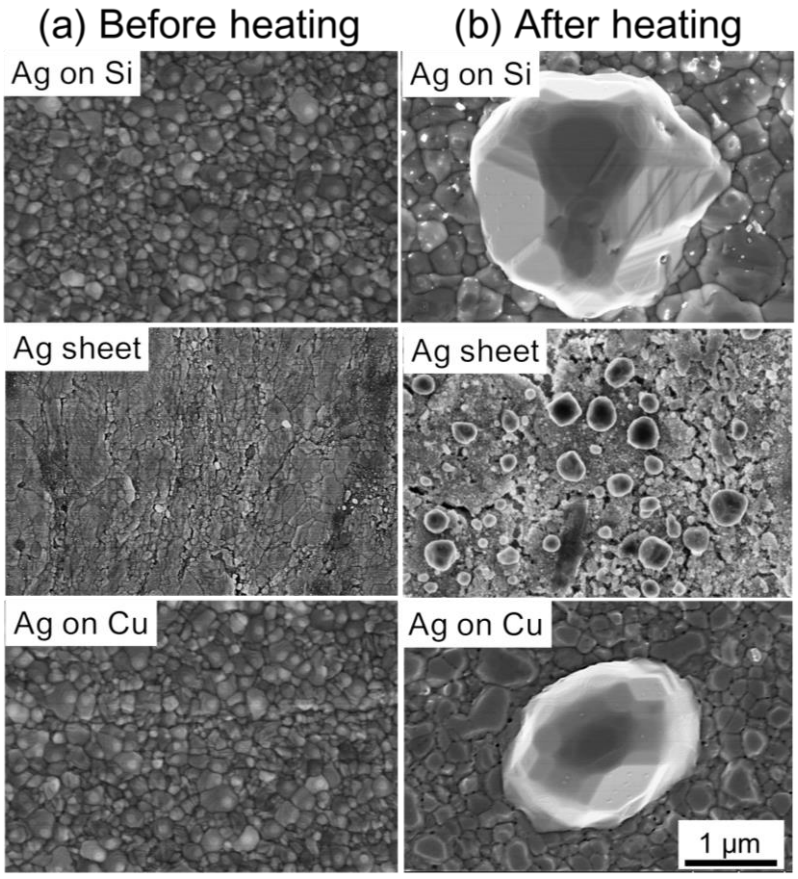

Fig. 3.2 Surface morphology of the Ag films and cold-rolled Ag sheet (a) before heating and (b) after heating at 250 ℃.

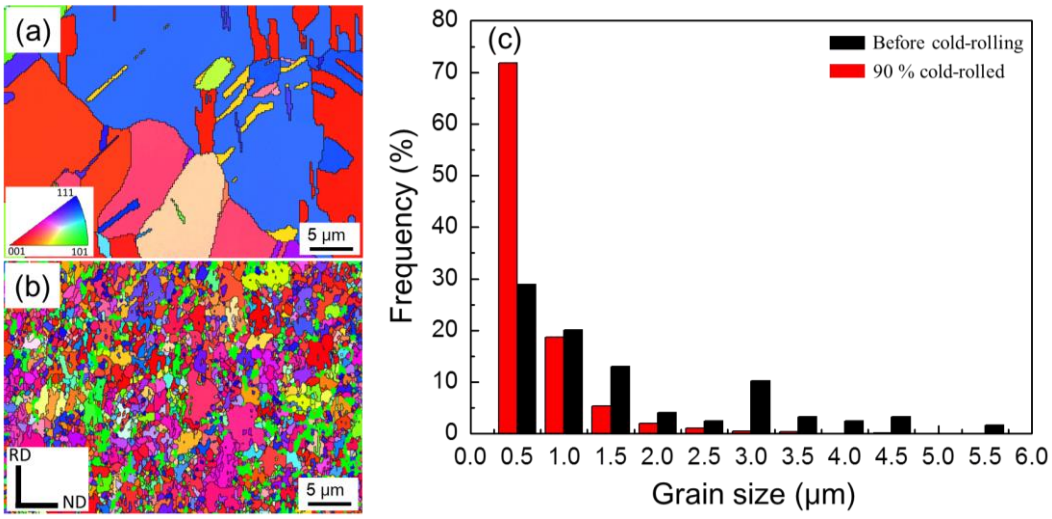

Fig. 3.3 EBSD (inverse pole figure) maps of the Ag sheet (a) as-cold-rolled and (b) 90% cold-rolled. Grain-size distribution (c).

3.3.2 Changes in microstructural evolution and bonding properties with rolling reduction ratio

Fig. 3.4 shows the surface morphology of Ag sheets with various reduction ratios after heating at 300°C. Fig. 3.4a shows a surface morphology of initial Ag sheet after heating, featuring flat surface without any hillock formation. With increasing rolling reduction in thickness, tiny hillocks were observed on the surface of cold-rolled Ag sheet after heating, as shown Fig. 3.4b and c. When the cold-rolling was conducted to a 90 % reduction in thickness, the largest size of hillock was observed among all specimens, as shown Fig. 3.4d.

The evolution of microstructure during cold-rolling was observed, as shown in Fig. 3.5. Before cold rolling, the average grain size of Ag sheet was about 4.82 μm, as shown in Fig. 3.5a. After cold rolling, the grain size decreased from the micro-scale to sub-micro-scale, resulting in increasing of grain boundary density (Fig. 3.5b and c). When the cold-rolling was conducted to a 90 % reduction in thickness, average grain size decreased up to 0.32. It has been reported that Ag grain boundary plays a key role in the formation of hillocks [16]. Thus, increasing the reduction ratio induced grain refinement down to a submicron level, which leads to the increasing of pathway to migrate Ag atoms along the grain boundary, resulting in a larger hillock formation.

The correlation between hillocks size and shear strength with various reduction ratios were evaluated, as shown in Fig. 3.6. With increasing reduction ratio, the hillock size increased. This result agrees well with the evolution of microstructure after heating (Fig. 3.4). The die-attach structure bonded with cold-rolled Ag sheet was achieved even using initial Ag sheet that did not form hillock after heating (Fig. 3.4a). This behavior is attributed to the hillock growth on the surface of Si and Cu substrate coated by Ti/Ag metallization layers. With increasing rolling reduction in thickness, the shear strength of the bonded specimens

increased to about 20 MPa by using the cold-rolled Ag sheet with 90% reduction ratio. The results indicate that contact interface between Ag sheet and substrates can be well bonded together when large quantity of hillock formed on the surface, leading to a solid-state bonding interface.

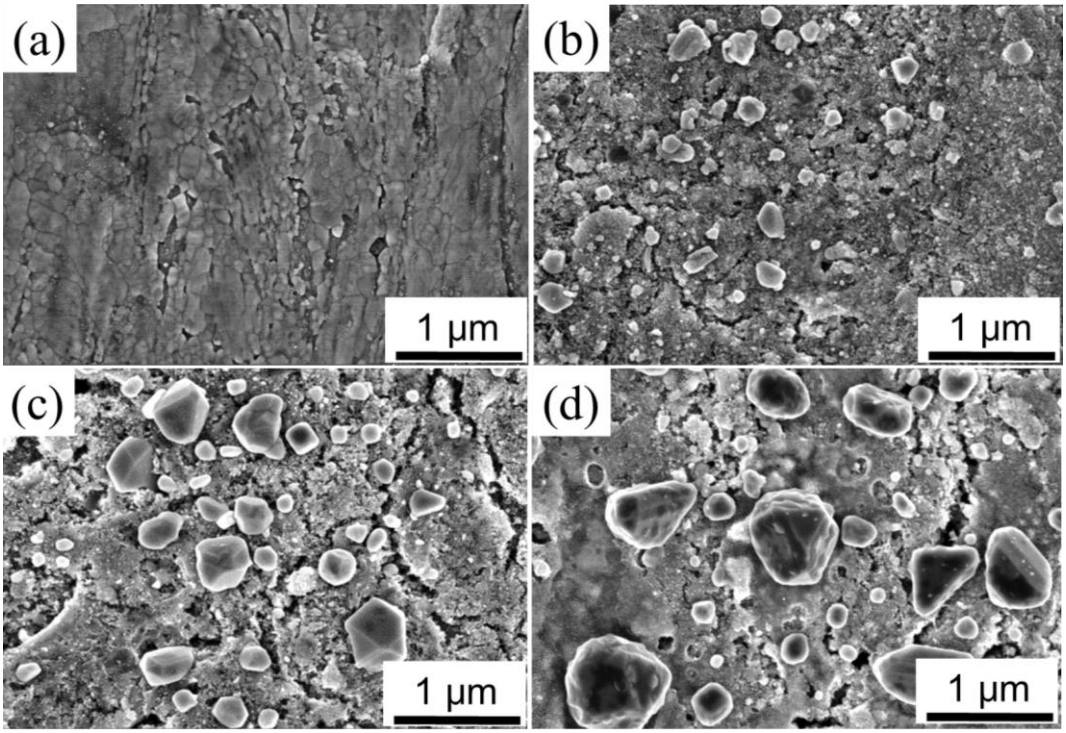

Fig. 3.4 Surface morphology of Ag sheets with various reduction ratios after heating at 300 °C: (a) 0 %, (b) 66 %, (c) 80 %, and (d) 90 %.

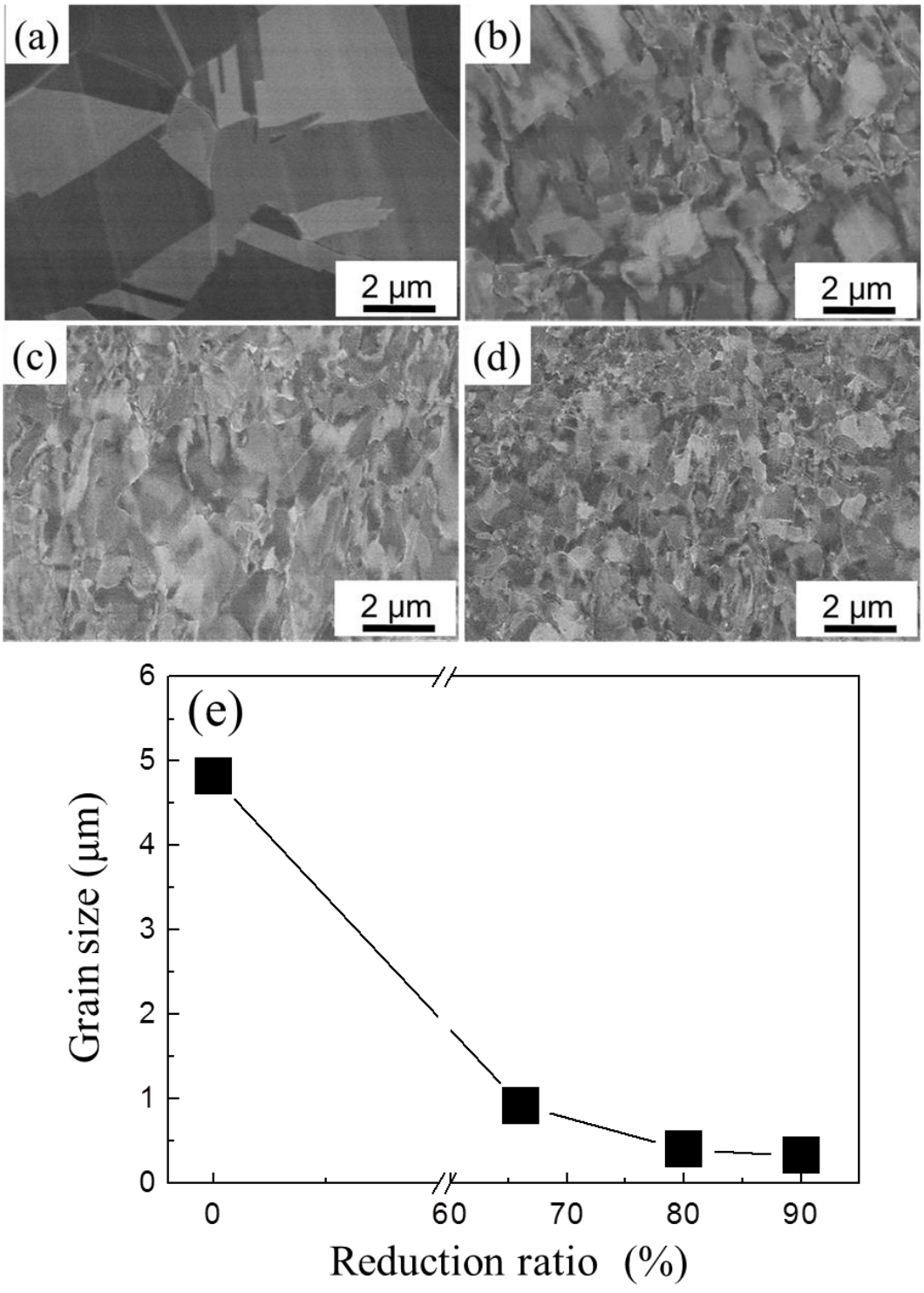

Fig. 3.5 Microstructure evolution of Ag sheets with various reduction ratios: (a) 0 %, (b) 66 %, (c) 80 %, and (d) 90 %. Variations in grain size (e).

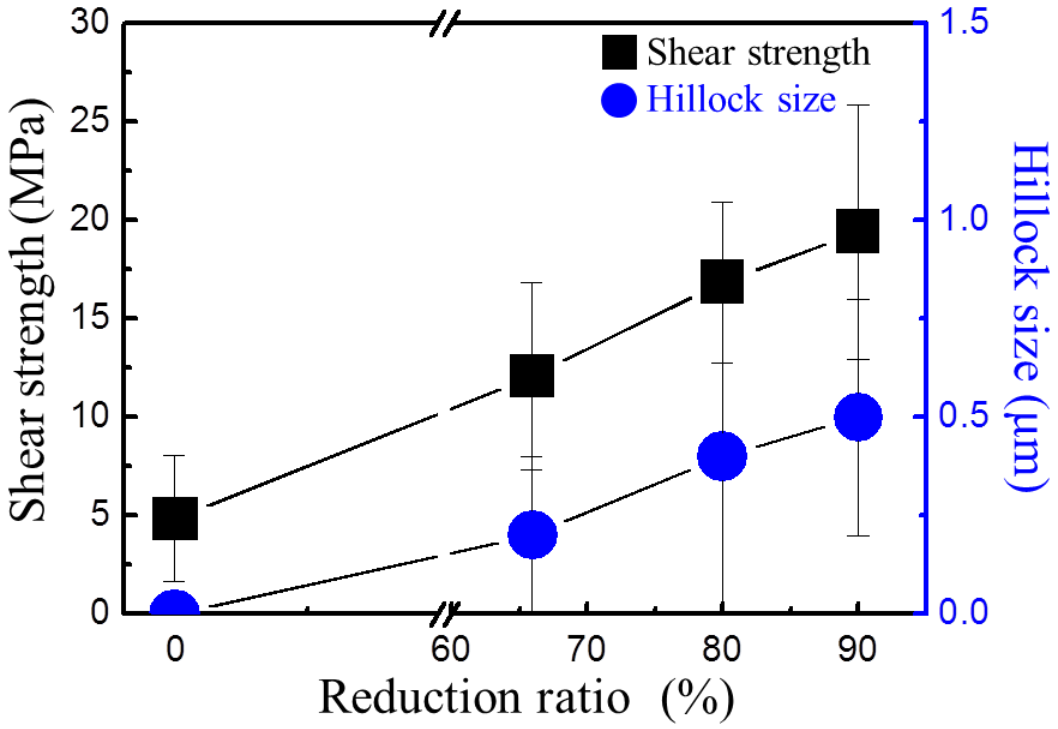

Fig. 3.6 Correlation between hillocks size and shear strength with various reduction ratios.

3.3.3 Changes in microstructural evolution and bonding properties with bonding temperature

Fig. 3.7a shows the results of the average die shear strengths at various bonding temperatures for a heating time of 1 h. The scattering in the shear strength is likely due to the non-uniform contacts between the samples, which is caused by the surface roughness of the materials. The die-attach structure bonded with a Ag sheet was achieved even at a low bonding temperature of 250 °C. The shear strength increased to 20 MPa at 300 °C and then decreased to 13 MPa at 400 °C. Fig. 3.7b and c show the SEM images of the cross section of the sputtered Ag/Ag sheet interface on the Si chip side and the Cu substrate side after heating at 250 °C, respectively. A part of the interface was bonded together by hillock growths, resulting in the achievement of solid-state bonding. The sputtered Ag/Ag sheet interface was completely bonded together at a bonding temperature of 300 °C, as shown in Figs. 3.7d and e. On the other hand, large voids appeared at the interface between the Ag sheet and the sputtered Ag film at higher bonding temperatures (Figs. 3.7f–i).

Fig. 3.8 shows how the microstructure of the cold-rolled Ag sheets changed after heat treatment for 1 h at various temperatures. In sheets heated at 300 °C, the optimum bonding temperature, we observed massive hillock growth. The decreased bonding interface at higher bonding temperatures (Fig. 3.7 f–i) are caused by less hillock formation at the surface, as shown Fig. 3.8c, b. This behavior can be explained by lateral grain growth in the Ag sheets was more dominant than hillock growth [17]. The decreased contact interface area of the Ag sheet and substrate, thus moderates the die- shear strength.

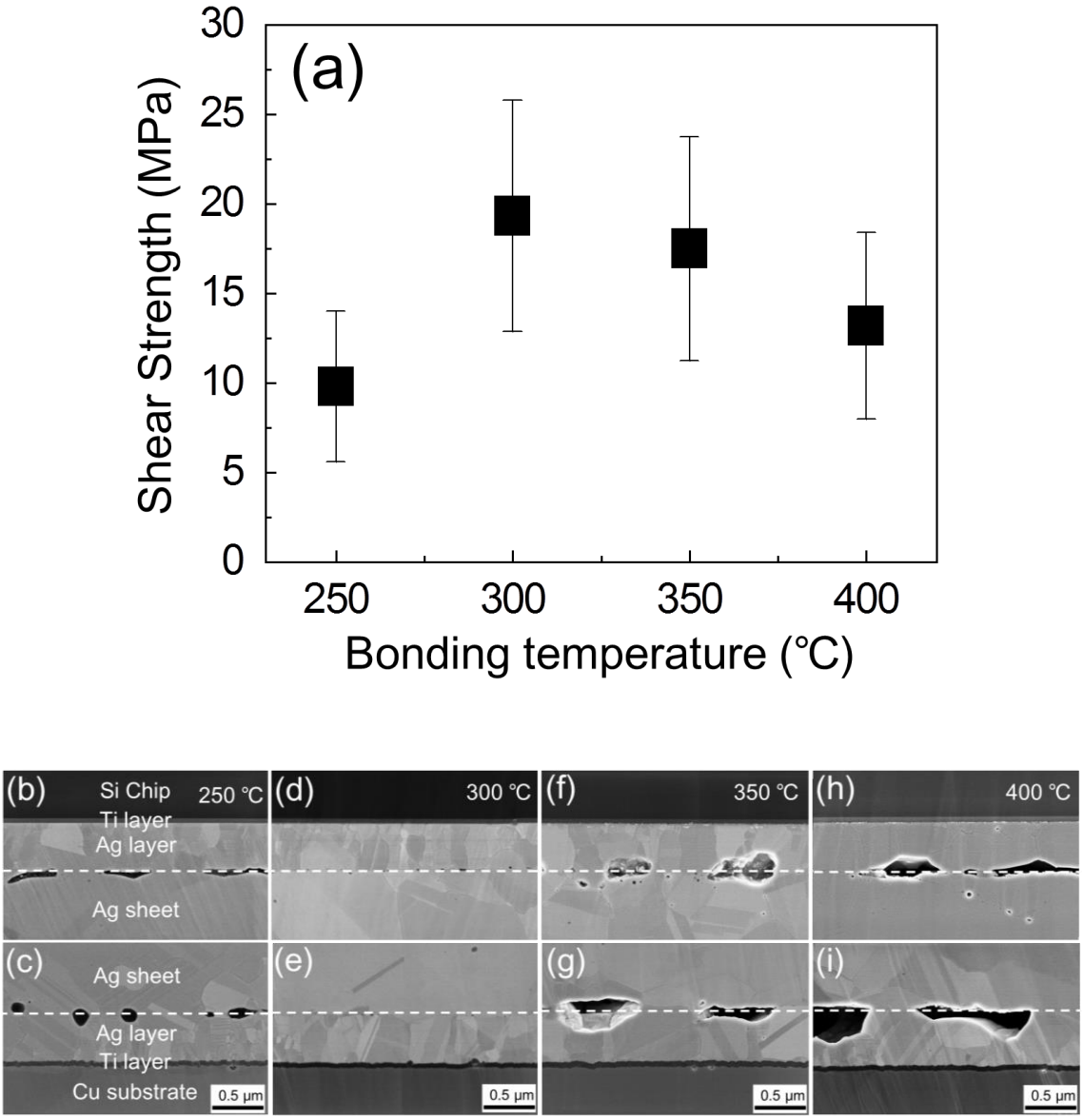

Fig. 3.7. Results for the average die shear strength at different bonding temperatures (a), cross-sectional SEM image of SMB using a cold-rolled Ag sheet bonded at different temperatures: (b, c) 250 °C, (d, e) 300 °C, (f, g) 350 °C, and (h, i) 400 °C.

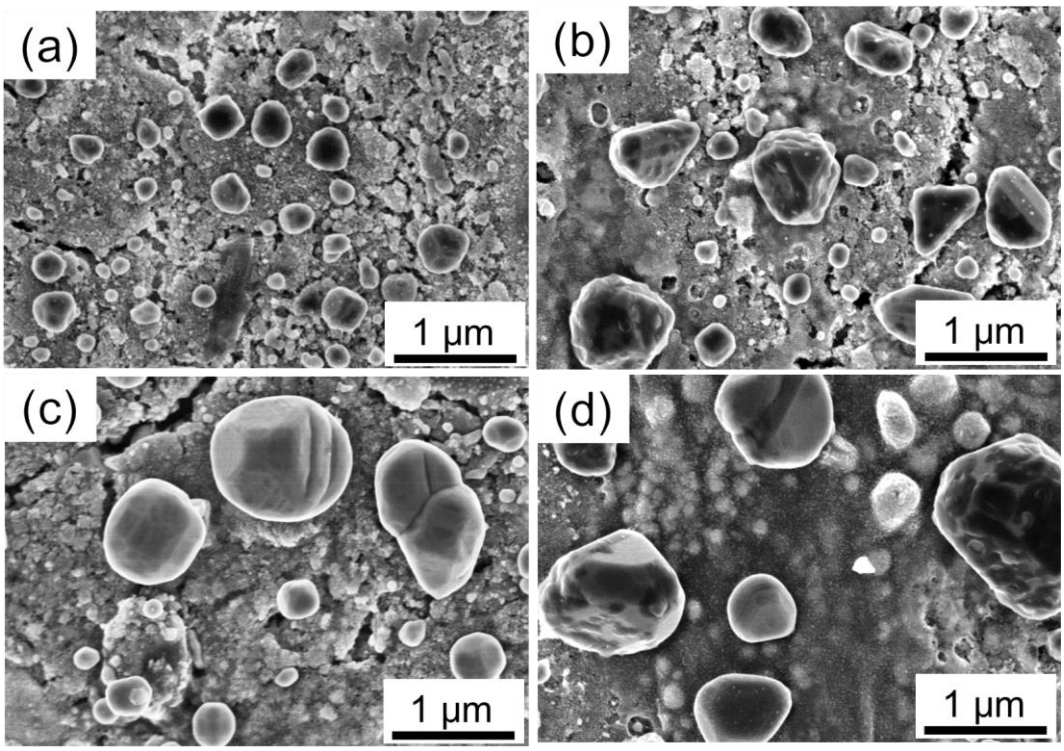

Fig. 3.8 Surface morphology of the microstructural evolution of cold-rolled Ag sheets at various bonding temperatures: (a) 250 ℃, (b) 300 ℃, (c) 350 ℃, and (d) 400 ℃.

3.3.4 Bonding mechanism

In this study, because the size of the hillocks on the Si chip was the largest among those for all the specimens (Fig. 3.2), we sputtered the Ag thin film on two Si substructures and mounted them together to fabricate a Si/Ag/Ag/Si joint structure and investigated the bonding mechanism between two hillocks via TEM. Fig. 3.9a shows a TEM image of the cross section between the two sputtered Ag thin films. A large quantity of Ag nanoparticles (AgNPs) formed and filled the gap between the two hillocks. In the meantime, a liquid-like microstructure was found around these AgNPs. Fig. 3.9b presents an amplified view of the local AgNPs. The size of most of AgNPs was <10 nm. A selected-area electron diffraction (SAED) pattern revealed that the AgNPs had a polycrystalline structure (Fig. 3.9c). Fig. 3.9d shows the SAED pattern for the liquid-like material around AgNPs, which indicates that the liquid-like phase has an amorphous structure. The amorphous structure mainly consists of O and Ag, as determined by energy-dispersive X-ray spectrometry.

In previous studies, it was reported that Ag–O fluids are formed by a specific reaction between Ag and O at the grain boundary of the Ag thin film and suggested that the amorphous layer is formed on the surface by the ejection of Ag–O fluids [20]. AgNPs were formed owing to the crystallization and decomposition of the Ag–O fluid along with the grain boundary when the compression stress achieved a constant value. In this study, the AgNP growth direction on the surface of the Ag grains was observed via TEM, as shown in Fig. 3.9e. Fig. 3.9f and g show a gradually amplified view of the local area of Fig. 3.9e. The AgNPs were regularly arranged on the surface and exhibited a specific growth direction, gradually expanding from the surface of the Ag grains to the external space. The result agree well with the "nano-volcanic eruption" theory when the AgNPs are grown from the inside of the Ag film. In addition, the TEM image supported that the AgNP growth may be a continuous process

under high-temperature conditions owing to the crystallization and decomposition of the Ag–O fluid. The AgNPs have a high surface energy, which allows them to be accumulated together easily and thus bridge the two hillocks, leading to the interface bonding together between two Ag films.

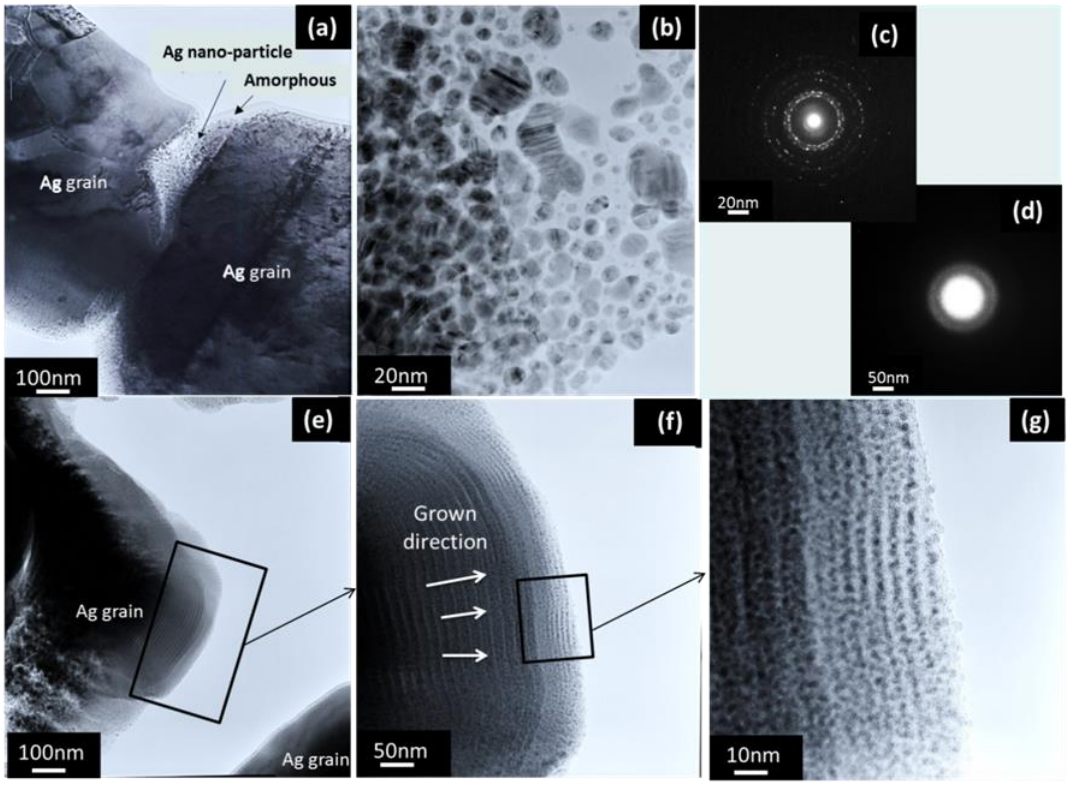

Fig. 3.9 TEM image of the Si/Ag/Ag/Si structure after annealing at 250 °C for 1 h in air (a); an amplified view of local area between the two Ag grains (b); SAED pattern of AgNPs (c) and the amorphous structure (d); AgNPs grown on the surface of Ag grains in a specific direction (e); and amplified view of the local area (f) and (g).

3.5 Conclusion

In summary, a bonding technology involving the use of cold-rolled Ag sheets is introduced for the die-attach structure. Hillocks can be formed on the surface of the Ag sheet via cold rolling owing to the relaxation of the residual stress generated during deformation. The structure of Si chip/Ag sheet/Cu substrate can be bonded together with generated hillocks based on the SMB. The die shear strength can reach 20 MPa at 300 °C. TEM observations confirm that the AgNPs were generated between two hillocks with a specified growth direction, where the AgNPs gradually expanded from the surface of Ag grains to the external space. Because AgNPs have a high surface energy, they can be accumulated together easily and thus bridge the two hillocks, leading to an interface between two Ag films bonded together. Because the Ag sheet has excellent properties with regard to thermal conductivity, electrical conductivity, and temperature stability, this bonding technology can serve as an alternative interconnection for WBG devices that require high thermal performance or extremely high operating temperatures.

References

[1] V. R. V. R. Manikam and K. Y. K. Y. K. Y. Cheong, "Die Attach Materials for High Temperature Applications: A Review," IEEE Transactions on Components, Packaging and Manufacturing Technology, vol. 1, no. 4, pp. 457–478, 2011.

[2] K. Suganuma, S. Sakamoto, N. Kagami, D. Wakuda, K. S. Kim, and M. Nogi, "Low-temperature low-pressure die attach with hybrid silver particle paste," Microelectronics Reliability, vol. 52, no. 2, pp. 375–380, 2012.

[3] P. Peng, A. Hu, A. P. Gerlich, G. Zou, L. Liu, and Y. N. Zhou, "Joining of Silver Nanomaterials at Low Temperatures: Processes, Properties, and Applications," ACS Applied Materials and Interfaces, vol. 7, no. 23, pp. 12597–12618, 2015.

[4] V. Caccuri, X. Milhet, P. Gadaud, D. Bertheau, and M. Gerland, "Mechanical Properties of Sintered Ag as a New Material for Die Bonding: Influence of the Density," Journal of Electronic Materials, vol. 43, no. 12, pp. 4510–4514, 2014.

[5] K. S. Kim, S. H. Huh, and K. Suganuma, "Effects of intermetallic compounds on properties of Sn-Ag-Cu lead-free soldered joints," Journal of Alloys and Compounds, vol. 352, no. 1–2, pp. 226–236, 2003.

[6] Y. Shi, J. Tian, H. Hao, Z. Xia, Y. Lei, and F. Guo, "Effects of small amount addition of rare earth Er on microstructure and property of SnAgCu solder," Journal of Alloys and Compounds, vol. 453, no. 1–2, pp. 180–184, 2008.

[7] Y. Yamada et al., "Pb-Free High Temperature Solder Joints for Power Semiconductor Devices," Transactions of The Japan Institute of Electronics Packaging, vol. 2, no. 1, pp. 79–84, 2009.

[8] M. S. Kim and H. Nishikawa, "Silver nanoporous sheet for solid-state die attach in power device packaging," Scripta Materialia, vol. 92, pp. 43–46, 2014.

[9] C. H. Sha and C. C. Lee, "Low-temperature solid-state silver bonding of silicon chips to alumina substrates," IEEE Transactions on Components, Packaging and Manufacturing Technology, vol. 1, no. 12, pp. 1983–1987, 2011.

[10] P. J. Wang, J. S. Kim, and C. C. Lee, "Direct silver to copper bonding process," Journal of Electronic Packaging, Transactions of the ASME, vol. 130, no. 4, pp. 450011–450014, 2008.

[11] P. J. Wang and C. C. Lee, "Silver joints between silicon chips and copper substrates made by direct bonding at low-temperature," IEEE Transactions on Components and Packaging Technologies, vol. 33, no. 1, pp. 10–15, 2010.

[12] S. K. Lahiri and O. C. Wells, "Reversible hillock growth in thin films," Applied Physics Letters, vol. 15, no. 7, pp. 234–235, 1969.

[13] S. J. Hwang, W. D. Nix, and Y. C. Joo, "A model for hillock growth in Al thin films controlled by plastic deformation," Acta Materialia, vol. 55, no. 15, pp. 5297–5301, 2007.

[14] D. K. Kim, W. D. Nix, R. P. Vinci, M. D. Deal, and J. D. Plummer, "Study of the effect of grain boundary migration on hillock formation in Al thin films," Journal of Applied Physics, vol. 90, no. 2, pp. 781–788, 2001.

[15] M. Kuramoto, T. Kunimune, S. Ogawa, M. Niwa, K. S. Kim, and K. Suganuma, "Low-temperature and pressureless Ag-Ag direct bonding for light emitting diode die-attachment," IEEE Transactions on Components, Packaging and Manufacturing Technology, vol. 2, no. 4, pp. 548–552, 2012.

[16] C. Oh, S. Nagao, T. Kunimune, and K. Suganuma, "Pressureless wafer bonding by turning hillocks into abnormal grain growths in Ag films," Applied Physics Letters, vol. 104, no. 16, 2014.

[17] C. Oh, S. Nagao, T. Sugahara, and K. Suganuma, “Hillock growth dynamics for Ag stress migration bonding,” Materials Letters, vol. 137, pp. 170–173, 2014.

[18] C. Oh, S. Nagao, and K. Suganuma, “Pressureless Bonding Using Sputtered Ag Thin Films,” Journal of Electronic Materials, vol. 43, no. 12, pp. 4406–4412, 2014.

[19] C. Oh, S. Nagao, and K. Suganuma, “Silver stress migration bonding driven by thermomechanical stress with various substrates,” Journal of Materials Science: Materials in Electronics, vol. 26, no. 4, pp. 2525–2530, 2015.

[20] S. Lin et al., “Nano-volcanic Eruption of Silver,” Scientific Reports, vol. 6, p. 34769, 2016.

[21] A. Njeh, D. Schneider, H. Fuess, and M. H. B. Ghozlen, “X-Ray residual stress gradient analysis in annealed silver thin films using asymmetric bragg diffraction,” A Journal of Physical Sciences, vol. 64, no. 1–2, pp. 112–122, 2009.

[22] S. Y. Lee, J. Ling, S. Wang, and J. Ramirez-Rico, “Precision and accuracy of stress measurement with a portable X-ray machine using an area detector,” Journal of Applied Crystallography, vol. 50, no. 1, pp. 131–144, 2017.

[23] D. Delbergue, D. Texier, M. Lévesque, and P. Bocher, “Comparison of Two X-Ray Residual Stress Measurement Methods : Sin 2 ψ and Cos α, Through the Determination of a Martensitic Steel X-Ray Elastic Constant,” Internal Conference on Residual Stresses 2016 (ICRS-10), vol. 2, pp. 55–60, 2016.

[24] M. Koç, J. Culp, and T. Altan, “Prediction of residual stresses in quenched aluminum blocks and their reduction through cold working processes,” Journal of Materials Processing Technology, vol. 174, no. 1–3, pp. 342–354, 2006.

Chapter 4

Large-area die-attach by stress migration bonding

4.1 Introduction

With the increasing demand for high-power density in power electronic systems, chip size becomes larger due to its larger current carrying capacity and lower impedance. The applications of large-area bonding (larger than 10 x 10 mm^2) in electronic systems such as insulated gate bipolar transistor and light emitting diode have grown considerably for the higher performance and lower cost. After the joining process in large-area die attach by Ag sintering paste, however, organic solvents were unexpectedly left inside the joint due to the lack of air circulation [10]. Such residual organic solvents can induce large voids or gaps in the joint area. For large bonding areas, high stresses could lead to a growth of cracks and voids during sintering process [11]. As a result, a decrease of the die shear strength has been observed for larger joint areas.

As mentioned in *Section 1.2.2*, two Ag-sputtered Si wafer can be bonded together at low temperatures by the abnormal growth of Ag hillocks, which is referred to as Ag stress migration bonding (SMB) [12–14]. Therefore, the Ag SMB process is expected to be applied in a large area die-attach for next-generation power devices. This chapter examines a bonding technology based on SMB process for large area die-attach. In order to ensure that the Ag SMB technique can be used for large area, the distribution of bonding strength of various spots was investigated on a substrate with the size of 20 × 20 mm^2. The reasons for strength fluctuations large areas were discussed for various positions ranging from center to edge.

4.2 Experimental

4.2.1 Materials and bonding process

SiO^2 substrates with a size of 20 mm × 20 mm × 10 mm were prepared for large area bonding. Before metallization layers were sputtered, the surface of substrate was cleaned via ultrasonication in acetone for 5 min. As adhesion layer, a 0.1 μm Ti metallization layer was deposited by radiofrequency sputtering. Subsequently, an Ag metallization layer with a thickness of 1.0 μm was deposited by direct-current sputtering, as shown in Fig. 4.1a. After cleaning in acetone for 5 min, two SiO^2 substrates with sputtered metallization layers were mounted at their Ag metallized sides. The mounted substrates were then placed on a hot plate and heated in air for 1h with an aided pressure of 0.1 MPa, as shown in Fig. 4.1b. The bonding temperatures were varied from 275 °C to 400 °C to find the optimum bonding condition that can produce the highest bonding strength. To study the spatial variations of the SMB process, one quarter of the bonded specimen was cut into 9 small specimens with an area of 3 × 3 mm^2, as shown in Fig. 4.1c.

4.2.2 Characterization methods

The bonding strength at various positions was measured by three point flexure tests at a loading rate of 0.001 m/s, as shown in Fig. 4.2a. A scheme view of the three-point flexure test is shown in Fig. 4.2b. Five bonded specimens were tested for each bonding condition. Scanning electron microscopy (SEM) was used to observe how hillock growth on the surface of the Ag metallization layer changed with the bonding conditions. The cross sectional microstructure was observed to assess how hillock growth is related to bonding strength. The size and number of the hillocks were calculated within a 20 μm × 25 μm area by analysing SEM images. In-situ the evolution of residue stresses in the Ag layer during heating was

measured by X-ray diffraction (XRD) by using the two-exposure method [16, 17]. Because the sputtered Ag layer exhibited highly {111} orientation [18], which is parallel to the surface of the substrate, the residual stress in the Ag layer can be evaluated by the two-exposure method with getting the lattice strains for (333) diffraction at $\psi = 0°$ and 70.5° determined by the relation of crystallographic orientation. The (333) diffraction peak at $2\theta = 156.87°$ was selected for the stress measurement with using monochromatic Cu Kα1 radiation generated at 40 kV and 30mA.

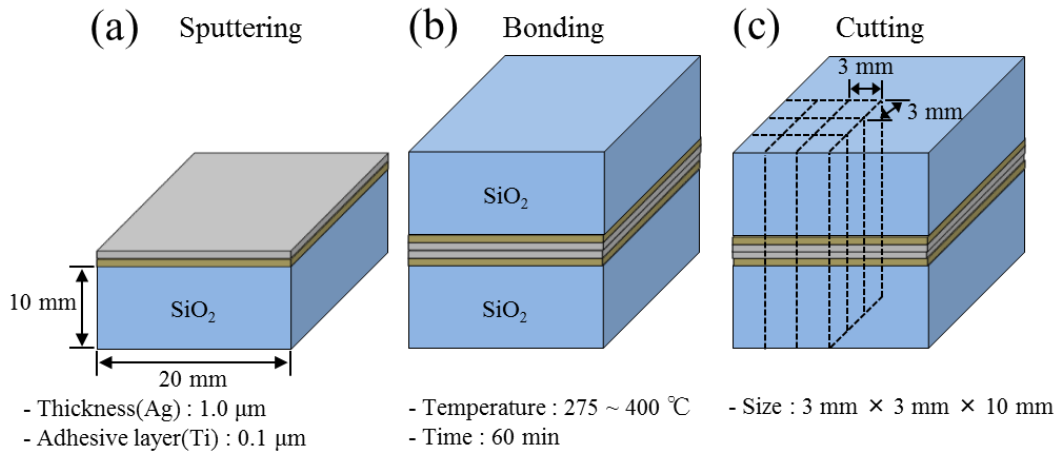

Fig. 4.1 Schematic of the experimental process: (a) sputtering, (b) bonding, and (c) cutting.

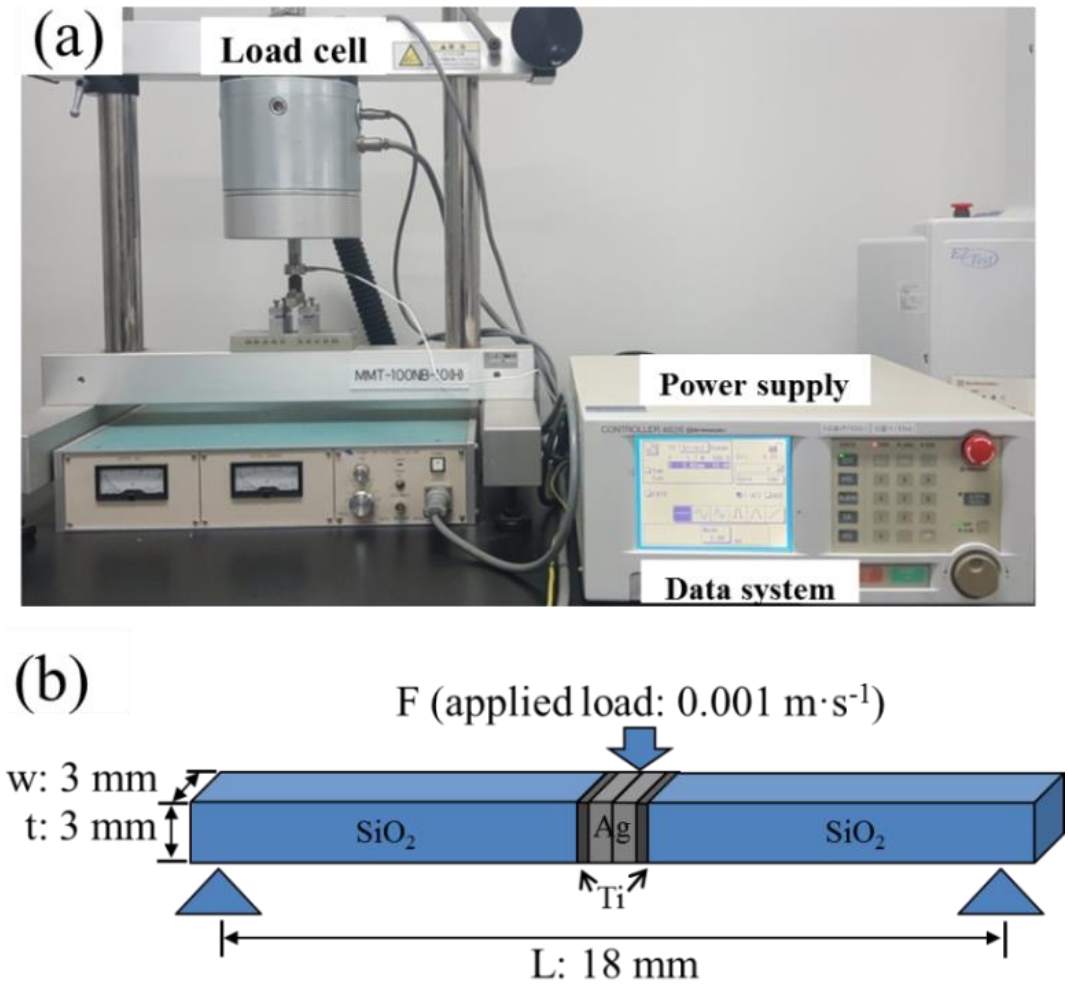

Fig. 4.2 Schematic of the three point flexure test: (a) three point flexure test setup and (b) specification of the specimen.

4.3 Results and discussion

4.3.1 Hillock formation and bonding properties with bonding temperature

Fig. 4.3a shows the average flexural strengths for all positions of the bonded specimen for various bonding temperatures. The scattering in the flexural strength is possibly from the non-uniform contacts caused by thermal warpage of the substrates. Large area bonding using Ag SMB was successfully achieved at low bonding temperature of 275 °C. With an increasing bonding temperature, the flexural strength increased to maximum of 40.5 MPa at 300 °C. Above 300 °C, it decreased to 22 MPa. Fig. 4.3b shows the cross-sectional microstructure of a bonding interface at 275 °C. The interface was partially bonded by hillock growth that filled interfacial gap between two substrates. A sound bonding interface was observed at bonding temperature of 300 °C, as shown in Fig. 4.3c. On the other hand, large voids formed at the bonding interface at higher bonding temperatures, as shown in Fig. 4.3d–f. The decreased flexural strength at higher temperatures was caused by such voids, which are formed by an accelerated Ag diffusion at high temperatures [19].

To verify the change of flexural strength and microstructures along with bonding temperatures, the hillock growth on the Ag layer was observed at various temperatures, as shown in Fig. 4.4. At a bonding temperature of 275 °C, small size of hillocks were observed on the Ag layer, as shown in Fig. 4.4a. The hillock growth represents a significant release of compressive stress caused by a large mismatch of CTE between the metallization and substrate [20, 21]. Fig. 4.4b shows a dense and large hillock growth on a Ag layer heated at 300 °C, which results in sound bonding joint (Fig. 4.3c). As the bonding temperature increased, the number of hillocks decreased, while voids sometimes formed, as shown in Fig. 4.4c, d. This behaviour can be explained when Ag metallization layer is continuously exposed to high temperatures over 350 °C, lateral grain growth in the Ag layer becomes more

dominate than hillock growth, causing the decreasing of driving force for stress migration toward the surface [22]. Thus, lake of driving force for hillock growth led to the voids in the bonding joint. These results well agree with the change of flexural strength and microstructures in bonding joints (Fig. 4.3).

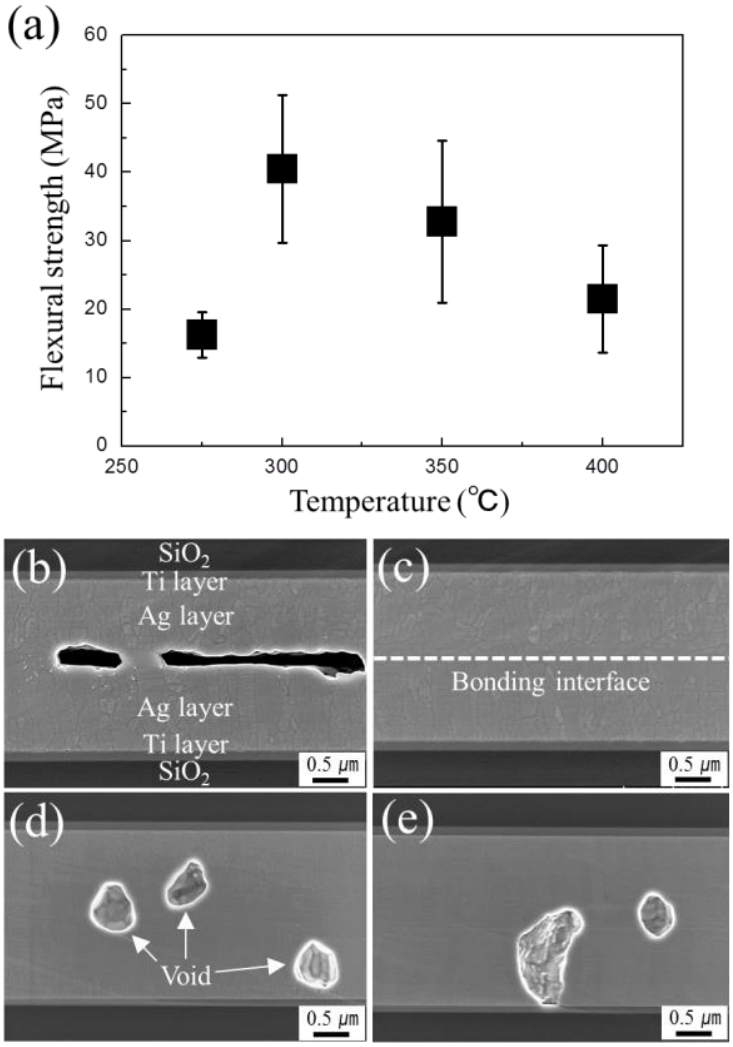

Fig. 4.3 (a) Flexural strength of specimens and cross-sectional SEM micrographs of the bonding interface at various bonding temperatures: (b) 275 ℃, (c) 300, ℃ (d) 350 ℃, and (e) 400 ℃.

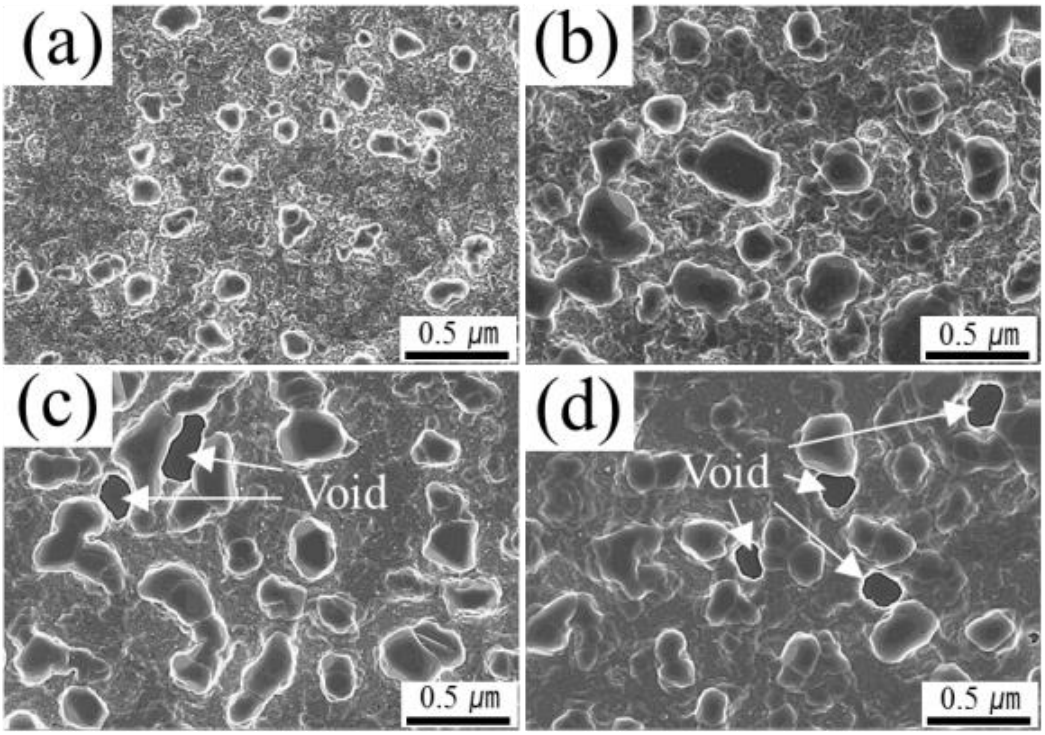

Fig. 4.4 Surface micrographs of the Ag layers at various bonding temperatures: (a) 275 ℃, (b) 300 ℃, (c) 350 ℃, and (d) 400 ℃.

4.3.2 Spatial variation in large area

To study the spatial variation in large area bonding, specimens bonded at 300 °C that showed highest bonding strength and sound bonding joints were evaluated with various positions, as shown in Fig. 4.5a. The highest flexural strength was obtained at the center of specimen while the edges showed the lowest strength. The largest difference of flexural strength value between the center and edge is 35 MPa. Fig. 4.5b and c show the SEM images of the cross section of interface at the center and the edge of the specimen after bonding at 300 °C, respectively. A sound bonding interface was observed at the center, as shown in Fig. 4.5b, while c shows that a gap between two Ag layers was partially formed, resulting in a decreased flexural strength at the edge.

In order to clarify the reasons for spatial variation of flexural strength, the hillock growth on the Ag layer surface was observed at the edge of the specimen, as shown in Fig. 4.6. At a bonding temperature of 300 °C, abnormal hillock growth was significantly scarce at the edge and the size of this area was about 700 μm from the edge, as shown in Fig. 4.6a. When a large amount of abnormal Ag hillocks occurred at the center (Fig. 4.6c), the interfacial gap between two Ag layers was completely filled by hillocks, resulting in a sound bonding joint. However, the hillock growth at the edges was relative weak and scattered compared to those at the center (Fig. 4.6d), resulting in a weak bonding between the Ag layers. We measured how the hillock growth changed after heating at 300 °C along with the area from center to edge, as shown in Fig. 4.7. Number list of the x-axis intercepts is shown in Fig. 4.5a. The average hillock size decreased, while the number of hillocks increased toward the edge, which indicates that the hillock growth and amalgamation was suppressed at the edges. We inferred that the spatial variation of the hillock growth can be attributed to the influence of an airflow near the edge. The airflow was induced by thermal convection during heating, which can penetrate inside the interface between two mounted Ag layers. Since the hillock growth is

nucleated from the eruption of Ag-O fluids during heating [15], its growth is easily affected by airflow that determines the distribution of the Ag-O fluids. In addition, the smaller space led to intensified convention. Since the edge part can only provide a rather tiny space for the air flow, the convention could be strong enough to disturb the growth and amalgamation of Ag hillocks at the edge.

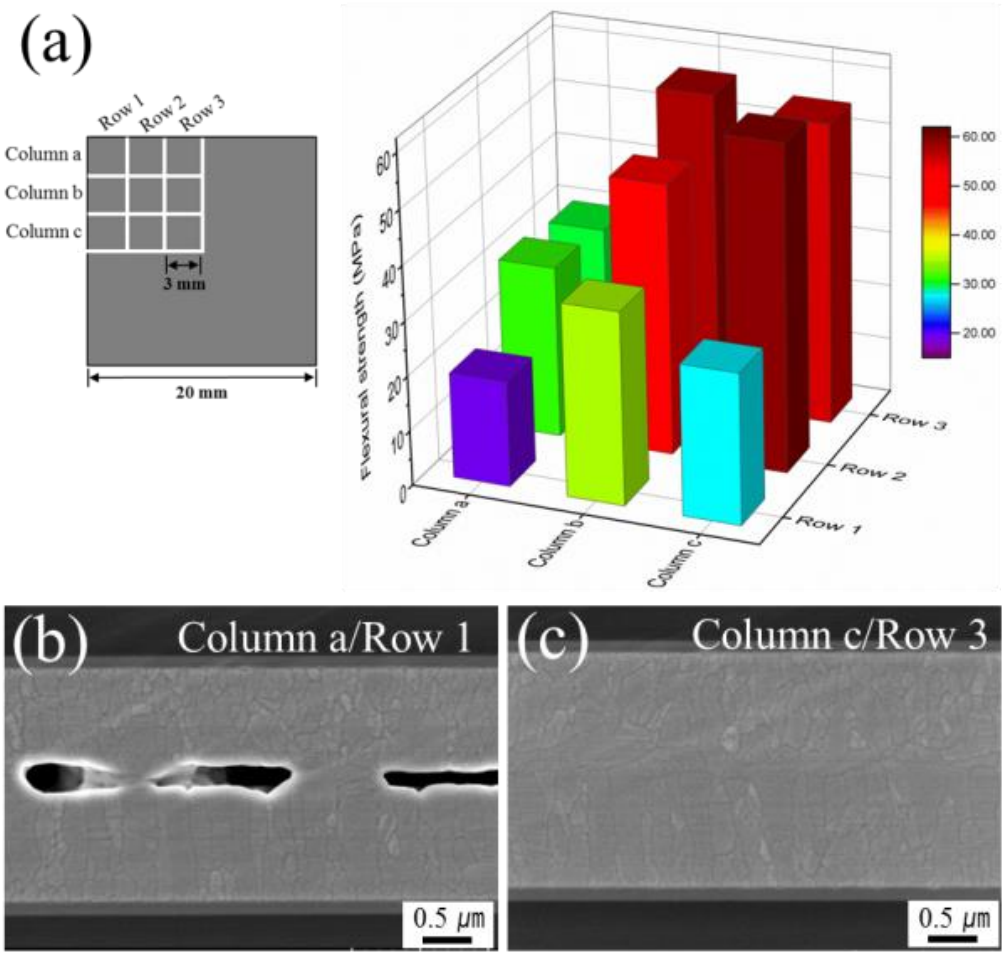

Fig. 4.5 Surface micrographs of the Ag layers at various bonding temperatures: (a) 275 °C, (b) 300 °C, (c) 350 °C, and (d) 400 °C.

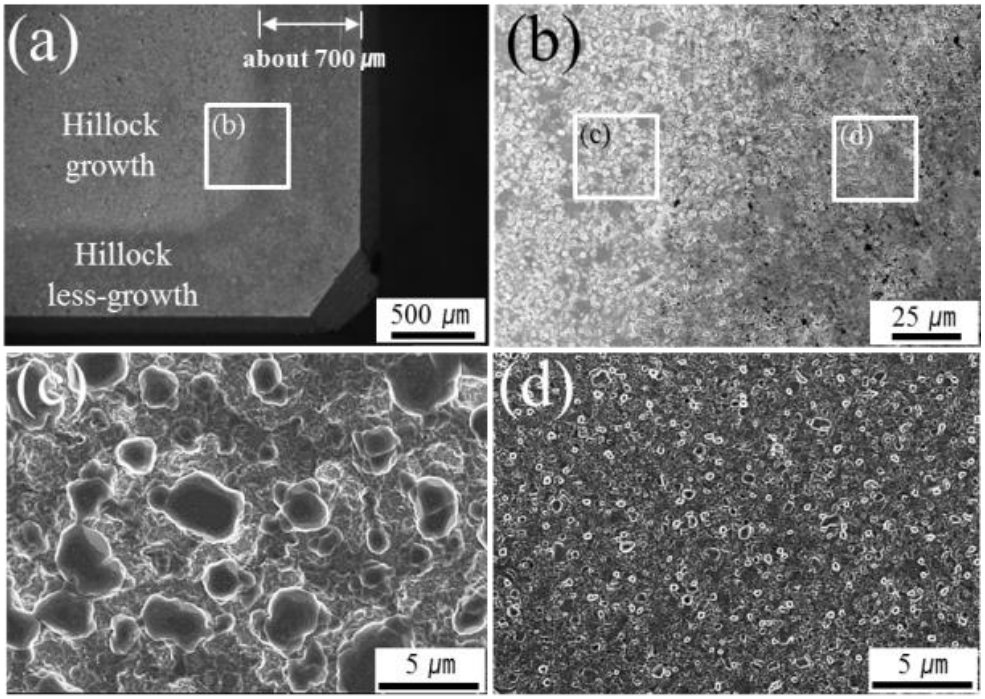

Fig. 4.6 The hillock growth after heating at the edge of the specimen (a) and its local enlarged view (b), (c) , and (d).

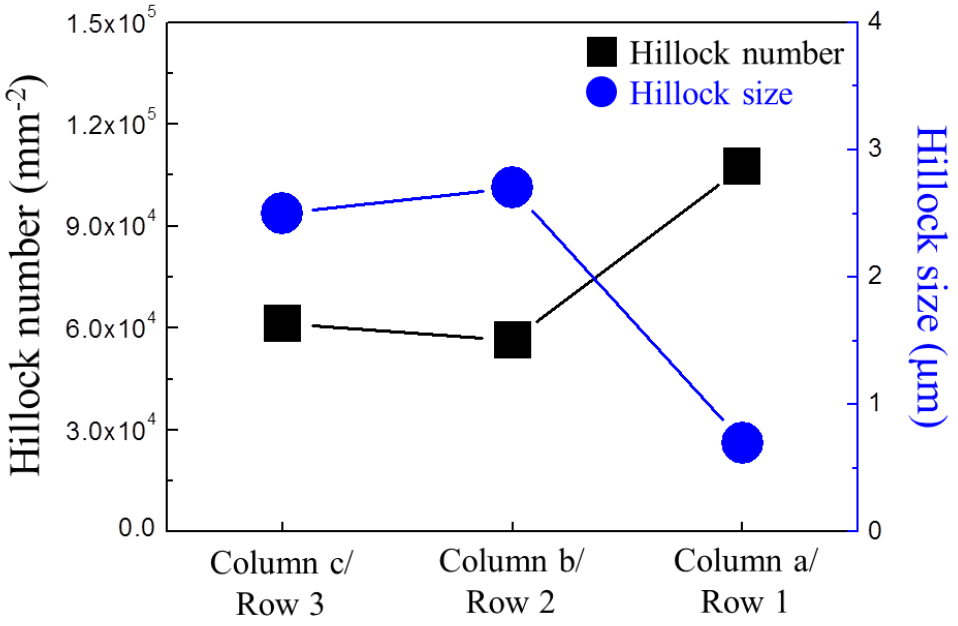

Fig. 4.7 Correlation of the size and number of hillocks after heating at 300 °C.

4.3.3 In-situ residual stress analysis

Since the compressive stress caused by the CTE mismatch at the Ag layer/substrate interface plays an important role in hillock growth, we measured the in-situ evolution of the residue stresses in the Ag layer during heating and cooling processes by XRD. Fig. 4.8a shows the evolution of the stress generated at the center, as numbered Row 3/Column c. The as-deposited Ag layer shows tensile residual stresses of about 60 MPa. With an increasing temperature, the tensile residual stress decreased to 10 MPa at 75 ℃ due to the compressive stress generated by CTE mismatch between Ag layer and substrate. The stress value decreased from the initial was about −55 MPa. Above 75 ℃, the residual stress increased, which indicates that concentrated compressive stress during heating was released by forming hillock on the surface of Ag layer. Fig. 4.8b and c show the evolution of stress generated at the Row 2/Column b and Row 1/Column a, respectively. The results showed the same tendency as observed for Row 3/Column c. The generated compressive stress due to CTE mismatch were released above 100 ℃ in all the specimens, which indicates that hillock growth occurred on the overall area.

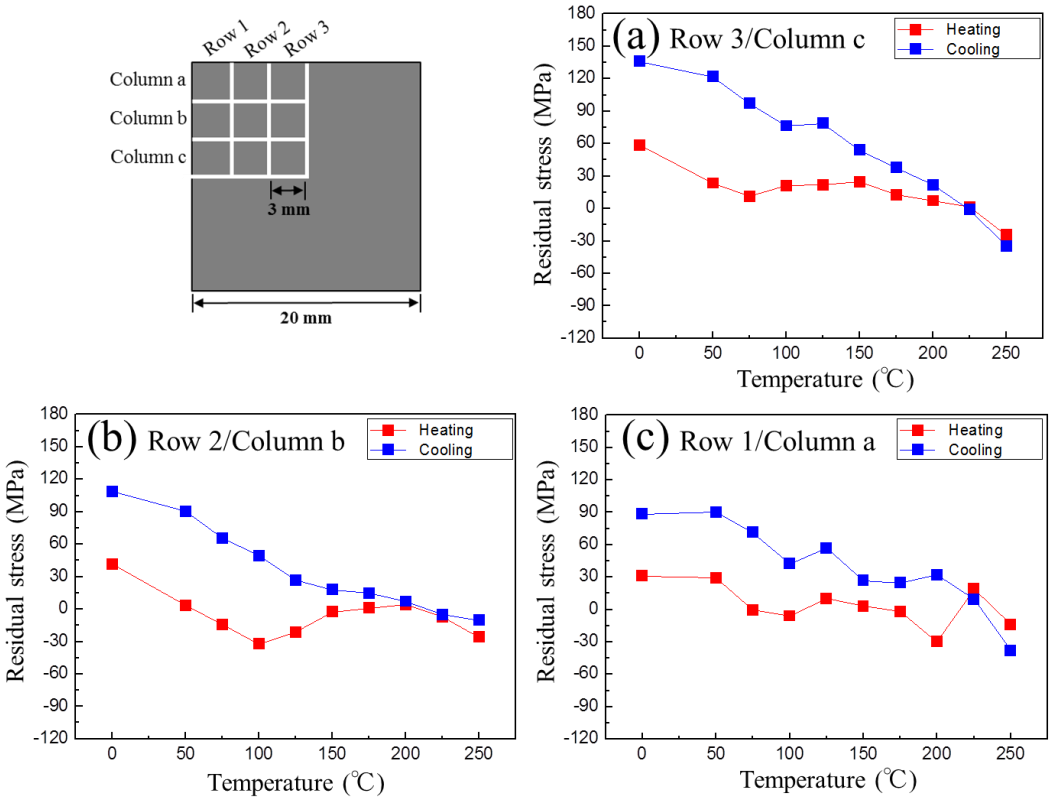

Fig. 4.8 In-situ stress analysis of Ag metallization layer by XRD (a) at Row 3/Column c, (b) at Row 2/Column b, and (c) at Row 1/Column a.

4.6 Conclusion

We demonstrated that Ag SMB technology can be used for large area die attach. By investigating the hillock growth at various temperatures and spots, we explained why the bonding strength varied. The large bonded area (20 x 20 mm^2) was achieved by using SMB technology, resulting in average flexural strength of 40.5 MPa at 300 °C. The formed hillocks have both a large volume and a dense distribution. The bonding strengths varied with the spatial variation of Ag hillock growth. A region with less hillock formation was found about 700 μm wide from the edge, which is caused by the intensified air flow. The in-situ measurements of the residue stresses were conducted by XRD and an obvious stress relaxation was observed from 100 °C and above, which attributes to the formation of abnormal Ag hillocks. The stress evaluation at different positions shows similar changing trends, which correspond well with the homogeneous hillock growth at the overall surface expect for the narrow edge areas. The shown bonding technology can be an attractive technology for large area bonding in the power device electronic applications and its reliability issue.

References

[1] M. S. Kim and H. Nishikawa, “Silver nanoporous sheet for solid-state die attach in power device packaging,” Scripta Materialia, vol. 92, pp. 43–46, 2014.

[2] K. Qi, X. Chen, and G.-Q. Lu, “Effect of interconnection area on shear strength of sintered joint with nano-silver paste,” Soldering & Surface Mount Technology, vol. 20, no. 1, pp. 8–12, 2008.

[3] T. Kunimune, M. Kuramoto, S. Ogawa, T. Sugahara, S. Nagao, and K. Suganuma, “Ultra thermal stability of LED die-attach achieved by pressureless Ag stress-migration bonding at low temperature,” Acta Materialia, vol. 89, pp. 133–140, 2015.

[4] M. Kuramoto, T. Kunimune, S. Ogawa, M. Niwa, K. S. Kim, and K. Suganuma, “Low-temperature and pressureless Ag-Ag direct bonding for light emitting diode die-attachment,” IEEE Transactions on Components, Packaging and Manufacturing Technology, vol. 2, no. 4, pp. 548–552, 2012.

[5] C. Oh, S. Nagao, T. Kunimune, and K. Suganuma, “Pressureless wafer bonding by turning hillocks into abnormal grain growths in Ag films,” Applied Physics Letters, vol. 104, no. 16, 2014.

[6] S. Lin et al., “Nano-volcanic Eruption of Silver,” Scientific Reports, vol. 6, p. 34769, 2016.

[7] T. Matsue, T. Hanabusa, and Y. Ikeuchi, “Residual stress and its thermal relaxation in TiN films,” Thin Solid Films, vol. 281–282, no. 1–2, pp. 344–347, 1996.

[8] Z. A. Khan, M. Hadfield, S. Tobe, and Y. Wang, “Ceramic rolling elements with ring crack defects - A residual stress approach,” Materials Science and Engineering A, vol. 404, no. 1–2, pp. 221–226, 2005.

[9] C. Oh, S. Nagao, and K. Suganuma, "Pressureless Bonding Using Sputtered Ag Thin Films," Journal of Electronic Materials, vol. 43, no. 12, pp. 4406–4412, 2014.

[10] S. Noh, C. Choe, C. Chen, and K. Suganuma, "Heat-resistant die-attach with cold-rolled Ag sheet," Applied Physics Express, vol. 11, no. 1, 2018.

[11] S. J. Hwang, W. D. Nix, and Y. C. Joo, "A model for hillock growth in Al thin films controlled by plastic deformation," Acta Materialia, vol. 55, no. 15, pp. 5297–5301, 2007.

[12] D. K. Kim, W. D. Nix, R. P. Vinci, M. D. Deal, and J. D. Plummer, "Study of the effect of grain boundary migration on hillock formation in Al thin films," Journal of Applied Physics, vol. 90, no. 2, pp. 781–788, 2001.

[13] C. Oh, S. Nagao, T. Sugahara, and K. Suganuma, "Hillock growth dynamics for Ag stress migration bonding," Materials Letters, vol. 137, pp. 170–173, 2014.

Chapter 5

Conclusions

In this thesis, novel heat-resistant interconnection materials, involving wire interconnection and die-attach, for WBG power devices were presented. Additionally, large-area die attach based on Ag stress migration bonding was proposed.

In chapter 1, the emerging issues, including the increase in demand for electric vehicles and their associated power electronic devices, were summarized. The recent research trends regarding packaging materials of power electronics that can endure extended exposure to severe service conditions as well as the research objectives of this study were also presented.

In chapter 2, a heat-resistant interconnection wire was introduced and manufactured by printing Ag sinter paste. The long-term reliability of Ag sinter paste wires was compared to Al ribbons by conducting harsh environmental tests such as an aging test at a temperature of 250 °C and an electromigration test at 2.2×10^4 A/cm^2. Serious conditions that gave rise to reliability problems were encountered at high temperatures, such as brittle intermetallic phases or interface corrosion. The resistance of APW did not increase significantly up to approximately 1000 h, and thereafter it increased only slightly over time as the EM test progressed. This proved that the resistance was considerably more stable than that of conventional Al ribbon bonding. The initial EM occurred mainly near the end of the joint between the APW and the Cu substrate, at which the maximum current density was observed. Subsequently, the von Mises stress accumulated along with Joule heating in the same location as the maximum current density, indicating that the crack caused by the shear stress may begin and propagate from the edge to center.

In chapter 3, a heat-resistant die-attach with cold-rolled Ag sheet was developed. Hillocks could be formed on the surface of the Ag sheet via cold rolling owing to the relaxation of the residual stress generated during deformation. The structure of the Si chip/Ag sheet/Cu substrate could be bonded together with generated hillocks based on the SMB. The

die shear strength could reach 20 MPa at 300 °C temperature. TEM observations confirmed that the AgNPs were generated between two hillocks with a specified growth direction, at which the AgNPs gradually expanded from the surface of Ag grains to the external space. Because AgNPs possess high surface energy, they can be gathered together easily and thus bridge the two hillocks, leading to an interface between the two Ag films that are bonded together.

Chapter 4 demonstrated that Ag SMB technology can be used for large-area die attach. By investigating the hillock growth at various temperatures and in various locations, an explanation was developed as to why the bonding strength varied. The large bonded area (20 × 20 mm) was achieved using SMB technology, resulting in an average flexural strength of 40.5 MPa at 300 °C. The formed hillocks possessed both a large volume and a dense distribution. The bonding strengths varied along with the spatial variation in Ag hillock growth. A region with less hillock formation was discovered, which was approximately 700 μm in width from the edge, and which was caused by the intensified air flow. In-situ measurements of the residue stresses were conducted by XRD and an obvious stress relaxation was observed from 100 °C and up, which was attributed to the formation of abnormal Ag hillocks. The stress evaluation at different locations showed similar changing trends, which corresponded well with the homogeneous hillock growth over the surface expect for the narrow edge areas.

Consequently, the demonstrated heat-resistant interconnection materials presented in this thesis can serve as alternative interconnection materials for WBG devices that require high thermal performance or can operate at extremely high temperatures. In addition, the Ag SMB process could be an attractive bonding technology for large-area die-attach.

List of publications

A. Papers

1. Chuantong Chen, **Seungjun Noh**, Hao Zhang, Chanyang Choe, Jinting Jiu, Shijo Nagao, and Katsuaki Suganuma, "Bonding technology based on solid porous Ag for large area chip" Scripta Materialia, 146 [15] (2018), 123–127.

2. **Seungjun Noh**, Chanyang Choe, Chuantong Chen, and Katsuaki Suganuma, "Heat-resistant die-attach with cold-rolled Ag sheet", Applied Physics Express, 11 [1] (2018), 016501_1–4.

3. **Seungjun Noh**, Chanyang Choe, Chuantong Chen, and Katsuaki Suganuma, "Printed wire interconnection using Ag sinter paste for wide band gap power semiconductors", Journal of Materials Science: Materials in Electronics, 29 [17] (2018), 15223–15232.

4. **Seungjun Noh**, Hao Zhang, Jeyun Yoem, Chuantong Chen, Caifu Li, and Katsuaki Suganuma, "Large-area die-attachment by silver stress migration bonding for power device applications", Microelectronics Reliability, 88 (2018), 701–706.

5. Chanyang Choe, **Seungjun Noh**, Chuantong Chen, Dongjin Kim, and Katsuaki Suganuma, "Influence of thermal aging upon mechanical and electrical properties of sintered porous silver during high temperature exposure", Microelectronics reliability, 88 (2018), 695–700.

6. **Seungjun Noh**, Hao Zhang, and Katsuaki Suganuma, "Heat-resistant microporous Ag die-attach structure for wide band gap power semiconductors", Materials, 11[12] (2018) 2531.

7. Chanyang Choe, Chuantong Chen, **Seungjun Noh**, and Katsuaki Suganuma, "Thermal shock performance of DBA/AMB substrates plated by Ni and Ni-P layer for high temperature applications of power device modules", Materials, 11[12] (2018) 2394.

8. Chuantong Chen, Zheng Zhang, Chanyang Choe, Dongjin Kim, **Seungjun Noh**, Toru Sugahara, and Katsuaki Suganuma, Improvement of bond strength of Ag sinter joining on electroless Au plated substrate by one step preheating treatment, Journal of Electronic Materials, 48[2](2019, 1106-1115.

B. Proceedings and Presentations

1. **Seungjun Noh**, Chuantong Chen, Shijo Nagao, and Katsuaki Suganuma, "Electromigration behavior in sintered Ag-paste wire bonding under high current density", 15th International Symposium on Microelectronics and Packaging (ISMP 2016), Seoul, Korea, October 24–26 (2016).

2. **Seungjun Noh**, Chuantong Chen, Toshiyuki Ishina, Shijo Nagao, and Katsuaki Suganuma, "Bonding technology for large area by silver stress migration bonding", 4th International Welding & Joining Conference 2017 (IWJC 2017), Gyeongju, Korea, April 11–14 (2017).

3. Chanyang Choe, **Seungjun Noh**, Toshiyuki Ishina, Shijo Nagao and Katsuaki Suganuma, "Thermal effect on material properties of sintered porous silver during high temperature ageing", 18th International Conference on Electronic Packaging Technology (ICEPT 2017), Harbin, China, August 16–18 (2017).

4. Chanyang Choe, **Seungjun Noh**, Toshiyuki Ishina, Chuantong Chen, Shijo Nagao and Katsuaki Suganuma, "Acoustic emission detection of Ag sinter joint failures of GaN power assembly", 161th annual meeting by the Japan institute of metal and materials, Sapporo, Japan, September 06–08 (2017).

5. **Seungjun Noh**, Chuantong Chen, Toshiyuki Ishina, Shijo Nagao, and Katsuaki Suganuma, "Printed Wiring for High-Power Electric Devices by Using Ag-sinter Paste", 50th International Symposium on Microelectronics (IMAPS 2017), Raleigh, USA, October 9–12 (2017).

6. Chuantong Chen, Aiji Suetake, Chanyang Choe, **Seungjun Noh**, Katsuaki Suganuma, "Low-stress Bonding Technology Design for SiC Power Die-attached Modules", 14th International Forum on Wide Bandgap Semiconductors 2017 (IFWS2017), Beijing, China, November 1–3 (2017).

7. Hao Zhang, **Seungjun Noh**, Norio Asatani, Yukiharu Kimoto, Aiji Suetake, Shijo Nagao, Tohru Sugahara and Katsuaki Suganuma, "A nearly-perfect Ag joints prepared by novel Ag to Ag direct bonding", 2018 Electronics Packaging and iMAPS All Asia Conference (ICEP-IAAC), Kuwana, Japan, April 17–21 (2018)

8. **Seungjun Noh**, Chanyang Choe, Chuantong Chen, Hao Zhang, and Katsuaki Suganuma, "Bonding technology using cold-rolled Ag sheet in die-attachment applications", International Power Electronics Conference (IPEC 2018), Niigata, Japan, May 20–24 (2018).

9. Chanyang Choe, **Seungjun Noh**, Chuantong Chen, Katsuaki Suganuma, "AE Evaluation of GaN Die-attach on DBC Substrate", 14th international ceramics congress (CITEC 2018), Perugia, Italy, June 04–08, (2018).

10. **Seungjun Noh**, Hao Zhang, and Katsuaki Suganuma, "Thermostable porous Ag die-attach structure for high-temperature power devices", International Symposium on 3D Power Electronics Integration and Manufacturing (3D-PEIM 2018), College Park, USA, June 25–27 (2018).

11. Hao Zhang, **Seungjun Noh**, Norio Asatani, Yukiharu Kimoto, Shijo Nagao and Katsuaki Suganuma, "Nearly perfect Ag joints prepared by Ag stress-migration-bonding (SMB) process", International Symposium on 3D Power Electronics Integration and Manufacturing (3D-PEIM 2018), College Park, USA, June 25–27 (2018).

12. **Seungjun Noh**, Hao Zhang, Jeyun Yoem, Chuantong Chen, Caifu Li, and Katsuaki Suganuma, "Large-area die-attachment by silver stress migration bonding for power device applications", 29th European symposium on reliability of electron devices, failure physics and analysis (ESREF 2018), Aalborg, Denmark, October 1–5 (2018)

13. Chanyang Choe, **Seungjun Noh**, Chuantong Chen, Dongjin Kim, and Katsuaki Suganuma, "Influence of thermal exposure upon mechanical/electrical properties and microstructure of sintered micro-porous silver", "29th Large-area die-attachment by silver stress migration bonding for power device applications", European symposium on reliability of electron devices, failure physics and analysis (ESREF 2018), Aalborg, Denmark, October 1–5 (2018).

Acknowledgment

I would like to express my sincere gratitude to my supervisor, *Prof. Katsuaki Suganuma*, for his support and academic guidance throughout my doctoral course. It was his steady support and inspiring guidance that brought this dissertation to its fruition. It was a great pleasure to conduct my work under his mentoring.

I would also like to appreciate members of doctoral committee, *Prof. Yoritoshi Minamino*, for insightful comments and helpful discussion for this dissertation. I would so like to appreciate *Assoc. Prof. Shijo Nagao* and *Assoc. Prof. Tohru Sugahara* for their valuable advices and encouraging comments during preparation activities of this dissertation. I am deeply grateful to *Assist. Prof. Chuantong Chen and Assist. Prof. Hao Zhang* for their unlimited support on my publication activities.

I would like to express the appreciation to members and alumni of Suganuma Laboratory, *Mr. Yukiharu Kimoto, Mr. Aishi Suetake, Mr. Yue Gao, Dr. Wanli Li, Mr. Jeyun Yeom, Mr. Chanyang Choe, Mr. Dongjin Kim, Dr. Jinting Jiu, Dr. Hao Zhang, Mr. Akio shimoyama*, for their kind support.

I would like to express the appreciation to my colleagues of Osaka University, *Dr. Minchan Jung, Mr. Wonrak Lee, Mr. Jungmin Kim, Dr. Pillgyu Choi, Ms. Jungin Kim, Ms. Sooyeon Jung, Mr. Hyoseok Si, Mr. Insung Choi, Ms. Jaebong Yeon, Dr. Gyeongtae Kim, Dr. Semin Park, Dr. Minsu Kim, Mr. Byungho Park*, for their warm encouragement and invaluable friendship.

Finally, I would like to express my sincere appreciation and love to my parents and brother, for their careful concern, moral support and dedication.